An Experimental Investigation of High-Shear-Strain-Rate Behavior of Metals

Thesis by
Nitin Deshpande

In Partial Fulfillment of the Requirements
For the Degree of
Aeronautical Engineer

California Institute of Technology
Pasadena, California
June 19, 1998

Acknowledgments

I would like to thank my advisor, Prof. G. Ravichandran, for his advice and support over the last year. I would like to express my appreciation to my friends Lavi Zuhal, Eric Burcsu, Benjamin Chow, Ioannis Chasiotis, Shiming Zhuang and Sandeep Sane for their constant support, advice, help and friendship. Thanks are also due to Ali Kiani, Joe Haggerty and Petros Arkelian for their help.

I would also like to thank Prof. Morteza Gharib and K. Bhattacharya for graciously agreeing to be on my thesis committee.

I am thankful to the Boeing Company for providing the financial support to carry out this study.

Abstract

The present study investigated the mechanical behavior of metals under high-shear-strain-rates and large shear strains. Numerical and experimental investigation of different specimen geometries for shear testing of materials was carried out. Results of numerical simulations showed that shear stress-strain curves calculated from boundary measurement of load and displacement did not match with the constitutive law for the material. The yield stress for the shear stress-strain curve from the boundary measurement was considerably lower than that of the constitutive law whereas hardening exponent was almost the same for two curves. Considerable bending was observed in the shear zone. The results from the boundary measurements were close to the constitutive law for H specimen, an analogue of axisymmetric top hat specimen with top replaced by tool steel punch. A planar version of axisymmetric top hat specimen geometry was studied using finite element analysis. The plane specimen was chosen since it is suitable for temperature measurements in the shear zone. In order to reduce the bending, three types of constraints were considered in the experiments.

Quasi-static and high strain rate experiments were carried out on different geometries in the strain rate range, 10^{-2} to 10^{4} s^{-1}. Relatively rate insensitive material, 2024-T3 aluminum was used to establish the relationship between numerical and experimental results. Experimental results for the axisymmetric top hat specimen were found to be in good agreement with the finite element results, but there was discrepancy between the stress-strain curve from the boundary measurements and the constitutive law. Shear stress-strain curve from the quasi-static test for the plane specimen with external constraint reproduced the results of numerical simulation. A planar specimen with built-

in constraint was fabricated using wire EDM. Both quasi-static and high strain rate results matched with the numerical simulation of the same specimen geometry. High shear strains of the order of 1.5 were reached in the experiments on the Kolsky pressure bar. Some amount of thermal softening was observed in high strain rate experiments.

It was concluded that both numerical simulations and experiments are required in order to obtain accurate constitutive behavior of the material using top hat specimen geometries. A relationship can be established between the numerical tests and the experiments by conducting the experiments at strain rates where the constitutive behavior of the metal is well known. This relationship then can be used to predict the constitutive law at higher strain rates from the experimental data obtained at high strain rates.

Table of Contents

Table of Figures

Chapter 1

Introduction

1.1 Motivation

It is well known that strain rate has considerable effect on the strength of the materials (e.g., Meyers, 1995). The responses vary widely, and it is therefore necessary to investigate individual materials to obtain the specific information regarding their constitutive behavior. For example, dynamic strength of some of the metals could be as high as twice its quasi-static strength. While stress-strain data at low strain rates is used in static problems, high strain rate behavior of the material is important in applications involving dynamic deformation and fracture.

There are a number of applications where dynamic deformation of metals is involved. The strain rates in orthogonal machining process are of the order of 10^4 s^{-1} to 10^5 s^{-1} (Marusich & Ortiz, 1995). Explosive welding is a process that involves very high strain rates in which two metal plates are placed on top of each other with specified spacing. The detonation of an explosive on top of the top plate propels it against the bottom plate at very high velocity and eventually forms a metallurgical bond between the two. This technology has been widely used to weld two metals, which cannot be welded using conventional welding methods. Another example where strain rates are very high is explosive metal forming. There are numerous military applications that are based on high strain rate behavior of metals. It is important to know the strength of the material at high strain rates for design of both penetrators and armor. There are two types of military

applications. One is the design of high velocity projectiles to defeat structures and the second is the design of armor that can protect these structures. Some of the examples of the projectiles include shaped charge, kinetic energy penetrator and explosively forged projectiles. An explosive charge placed in contact with a hollow metal cone detonates and deforms the cone into a long rod that is accelerated to velocities up to10 km/s. This "jet" has great penetration capability. A long cylindrical rod of high density metal traveling at a velocity of 1.5-2 km/s can penetrate into steel target to approximately one-half of its length. Design of armor is based on high-strength, lightweight, impact-resistant materials. There are other applications of high-strain-rate deformation, such as machining, accidental impact of vehicles and explosive devices. Some of the examples involving high strain rates in aerospace industry include shielding of space vehicles against micrometeorite impact and aircraft hardening to resist explosive loading. These applications require a thorough knowledge of the mechanics of high strain rate deformation and the dynamic response of the materials.

Other fields of scientific study, which require thorough knowledge of the high strain-rate properties of the metals, are adiabatic shear banding and dynamic fracture. Adiabatic shear banding is one of the predominant failure modes in many metals under high rates of deformation. The occurrence of shear bands at high strain rates is a thermomechanical process driven mainly by heat generated due to plastic dissipation at high-strain-rates (Zhou *et al.*, 1998). There is a considerable plastic deformation at the crack tip in ductile metals during dynamic fracture that leads to generation of heat. Consequently, a significant temperature rise can occur at a dynamically propagating crack tip propagating at high velocities (Zehnder & Rosakis, 1991).

Present experimental techniques can provide stress-strain data for only limited strain range (~ 0.5). Constitutive models for high strain rates for large strains and temperatures do not exist, and usually they are extrapolated. To understand and model various processes and applications described above, it is necessary to obtain stress-strain data at large strains and high strain rates. Knowledge of the accurate constitutive behavior of the materials for large strains and a wide range of strain rates is critical in computational modeling of the high speed machining process. Typical strain rates involved in high speed machining process are of the order of 10^4 s^{-1} to 10^5 s^{-1}. This process could be highly inhomogeneous and involves shear localization and fracture. Shear strains as high as 5 to 10 could prevail within the shear zones at the tip of the tool. It is difficult to make measurements of the properties such as stress, strain or temperature in the vicinity of the tool. Various computational codes have been developed to model these processes (e.g., Marusich and Ortiz, 1995), but the accuracy of these models depends on the constitutive law used as input to the code. Thus, reliable and accurate stress-strain data from the experiments for large strains, high strain rates and high temperatures is required if numerical simulations for these processes are to be realistic.

Fig. 1.1 shows schematic classification of testing techniques at different strain rates. At low strain rates, inertial forces are negligible and the specimen used in the test is under static equilibrium. At strain rates below 10^{-5} s^{-1}, visco-plastic response of metals is studied at elevated temperatures using conventional creep testing machines. Quasi-static testing of the materials for strain rates between 10^{-5} s^{-1} to 1 s^{-1} is done using servo-hydraulic or screw-driven testing machines. At higher strain rates, the Kolsky bar, the expanding ring and the Taylor test are used. The strain rates achieved in these tests are

between 10^3 s^{-1} to 10^4 s^{-1}. Kolsky bar is a relatively simple and widely used technique for intermediate strain rate testing (10^3 s^{-1}-10^4 s^{-1}) (Kolsky, 1949). There are different versions of this method, which can be used for tension, compression and torsion testing of the materials. The expanding ring technique is one in which an explosive is detonated at the core of the cylinder, which sends a shock wave through a metal ring that expands at high velocity. Stress-strain measurements in the ring using interferometric methods give high strain rate properties of the material. Pressure-shear plate impact is a relatively new procedure that is used to obtain shear stress-strain curves at strain rates from 10^5 s^{-1} to 10^6 s^{-1}. Pressure-shear impact testing is performed by impacting a thin, soft specimen with a hard, elastic flyer plate inclined at an angle with respect to specimen plate. The thin specimen is supported on a thick elastic anvil plate, which creates a state of high pressure and high shear strain-rate in the thin specimen. The stresses in the elastic plate are inferred by measuring the projectile velocity and the particle velocity at the rear surface of the anvil plate (ASM Handbook, Vol. 8). In the range 10^6 s^{-1} to 10^8 s^{-1}, shear wave and shock wave propagation are involved and this is achieved by high velocity impact, by the detonation of explosives in contact with the material, or by pulsed laser or other source of radiation. Some of the methods that use these techniques are listed in Fig. 1.1.

Although various well-established methods are available to obtain stress-strain data at different strain rates, there are some distinct strain rate regions for which data is missing because of the lack of reliable techniques. Two such ranges are from 10^0 s^{-1} to 10^3 s^{-1} and from 10^4 s^{-1} to 10^5 s^{-1}. Maximum strain-rates are limited to $5x10^3$ s^{-1} in the torsion configuration of the Kolsky bar. As will be discussed later, different specimen geometries can be used in the tests to obtain shear properties of the metals. Plate impact

methods can achieve much higher strain-rates; however, the test setup is quite complicated and usually involves interferometric techniques to measure stress. Furthermore, test samples are subjected to large pressure in addition to shear. This points to a need for a reliable experimental technique, preferably in shear, using which one can attain large strains and high strain rates. Such a technique could possibly provide a means to evaluate the material properties in the strain rate regimes otherwise unexplored, namely 10^1 s^{-1} to 10^3 s^{-1} and 10^4 s^{-1} to 10^5 s^{-1}. An important aspect of high-strain-rate deformation of metals is the fraction of plastic work converted to heat. Recent investigations (Mason *et al.*, 1994, Hodowany *et al.*, 1998) have determined the fraction of plastic work converted to heat in the strain rate regime, 10^3 s^{-1} to 10^4 s^{-1}, and found it to be a function of plastic strain and strain rate. Techniques such as the pressure-shear plate impact are not amenable to direct temperature measurement. It would be beneficial to develop a specimen geometry, which in addition to measuring the constitutive response would also be accessible for temperature measurements using established techniques such as the high-speed infrared thermography (Hodowany, 1997).

1.2 Previous Work

Various attempts have been made in recent years to obtain stress-strain relationship for metals under high shear strain rate. Meyer *et al.* (1981) developed a new axisymmetric hat-shaped specimen to study the properties of metals under localized shear at high strain rates. The specimen was used to produce controlled initiation and propagation of shear bands during Kolsky pressure bar testing. Since then, this geometry has been widely used by different investigators for studying shear behavior of metals. Beatty *et al.* (1992) used top hat specimens to study formation of adiabatic shear bands in

AISI 4340 high strength steel. They obtained stress-strain data for shear strain rates from 10^3 to $3x10^5$ s^{-1}. They also studied microcrystalline structure within shear bands using a TEM. Vecchio (1994a) studied high-strain, high-strain-rate deformation of tantalum and tantalum-tungsten alloys using hat-shaped specimens. This geometry was also used to observe microstructure of shear bands in Al-Li alloys by Vecchio (1994b). Minnaar and Zhou (1998) tested number of materials, HY-80, HY-100, HSLA-80, 4340 VAR and Ti-6Al-4V for their dynamic shear failure resistance. They also obtained shear stress-strain curves at different strain rates using top hat specimens. Chung *et al.* (1994) used finite element code with explicit time integration to study formation of adiabatic shear bands in top hat specimens. They included effects of strain hardening, strain-rate hardening and thermal softening in their material model. They conducted experiments on 4340 steel to verify the results of their numerical simulations.

There are modified versions of hat-shaped specimen that have been used for shear testing at high and very high strain rates. Klepaczko (1994) used MDS (modified double shear) specimen to obtain upper and lower yield stresses for low alloy steel XC18 at shear strain rates from 10^{-4} to $5x10^4$ s^{-1}. A new experimental technique based on direct impact of a long rod on MDS specimen supported by a Hopkinson tube was used. An optical extensometer was used for non-contact direct measurement of the shear strain. Numerical study of the deformation of MDS specimen was carried out and a calibration factor to correct the experimental data was suggested.

It is not known currently whether shear stress-strain curves obtained from the top hat specimen using boundary measurements could be used as the constitutive law for the material. Numerical study of MDS specimen suggests that the experimentally obtained

stress-strain response might be different from the actual response of the material. Also axisymmetric geometry does not allow for complete thermomechanical characterization of the material, i.e., does not allow for direct measurement of temperature. Thus, it is necessary to understand the relationship between load-displacement response of the specimen used in the experiments and the true constitutive behavior for the material and also develop a new specimen geometry that makes temperature measurements in the shear zone possible.

1.3 Objectives

The goal here was to develop a relatively simple technique, which would allow one to measure shear flow stress at higher strain rates by extending limits of the hydraulic material testing system and the standard Kolsky bar configuration. The strategy was to design a modified specimen geometry that could be investigated using the materials testing system (MTS) and the compression Kolsky bar.

In order to understand the limitations of the hat-shaped geometry commonly used in shear testing of metals, a numerical study was carried out. Results of this study are presented in Chapter 2. Comparison of these results with the constitutive law indicated that both numerical and experimental study is required to predict correct constitutive behavior of the material. Various new geometries were suggested and tested using finite element simulations. Planar version of hat-shaped specimen was found to give good numerical results. Various constraints were used to avoid excessive bending of the plane specimen. Finally, a planar hat-shaped specimen with built in constraint was found suitable for performing high strain rate experiments.

Experimental results for different geometries of the top hat specimen are presented in Chapter 3. Both quasi-static and high-strain-rate experiments were carried out on different specimens made from commercially available 2024-T3 aluminum. This material was found to be best suited for establishing relationship between computational and experimental results owing to its relative rate insensitivity (Hodowany, 1997). Shear stress-strain curves obtained from the experiments were compared with the numerical results. There was a good match between numerical and experimental results for the plane top hat specimen. Chapter 4 summarizes the conclusions of the present investigation and suggestions for future work are presented.

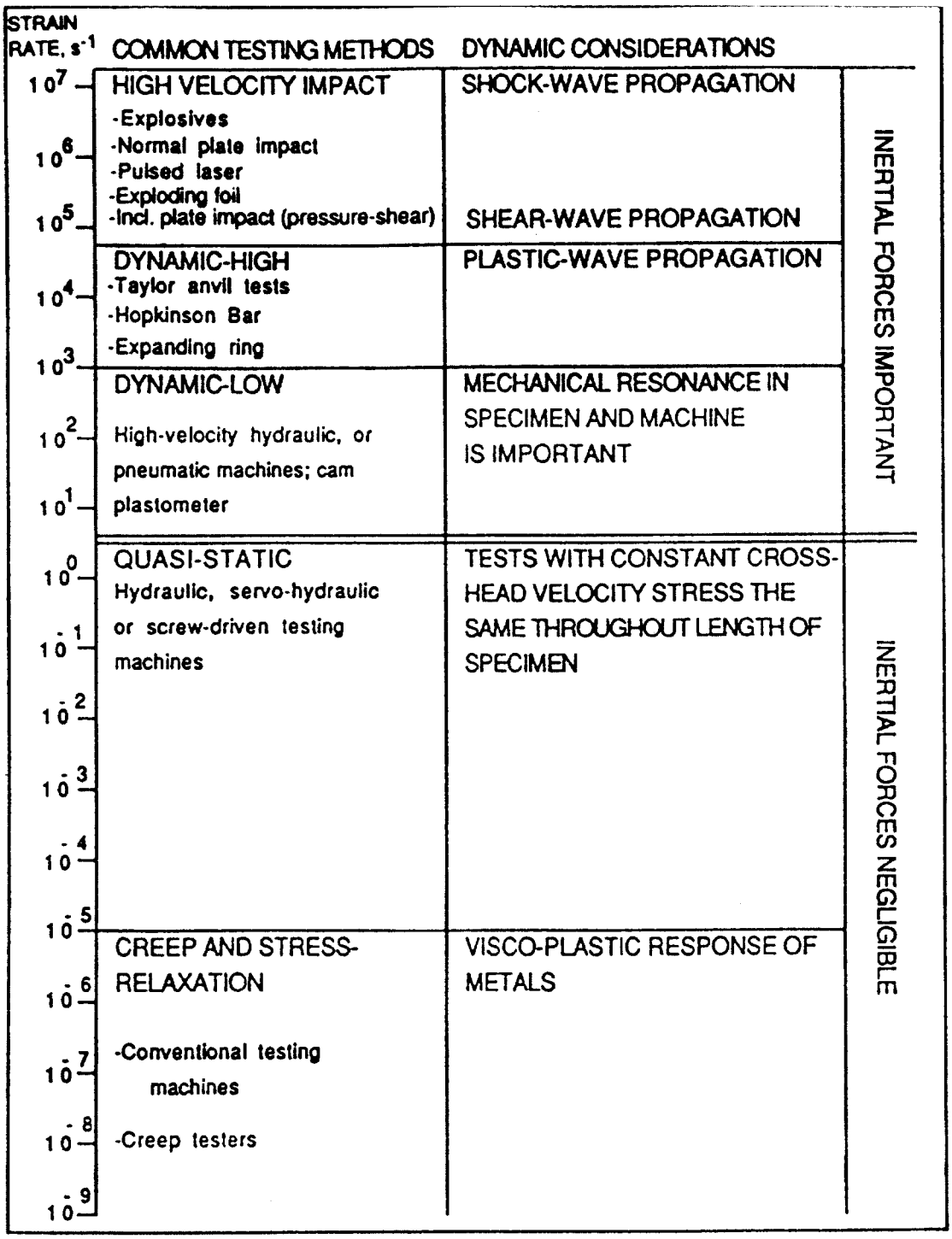

Figure 1.1 Schematic classification of testing techniques according to strain rate (From Meyers (1994))

Chapter 2

Theory and Simulations

2.1 Theory of Plasticity

Theory of plasticity can be illustrated using the uniaxial stress-strain response of a structural metal. From such a description, the constitutive law for plasticity can be constructed. It is well known that when a simple solid bar is subjected to tensile loading, there is stress level called yield stress beyond which the bar undergoes permanent deformation. Mathematically, in case of simple tension, $\sigma > \sigma_0$ is in the state of yielding and in simple shear, $\tau > \tau_0$. In case of multiaxial state of stress, the condition, which characterizes the transition of material from elastic state to plastic state is given by yield surface, a mathematical idealization of the extent of the elastic region. For an isotropic body this condition is a symmetrical function of principle stresses.

$$f(\sigma_1, \sigma_2, \sigma_3) = K = const. \tag{2.1}$$

where σ_1, σ_2, σ_3 are principle stresses.

There are various theories, which formulate different conditions for onset of plasticity. Tresca-Saint Venant condition is based on constant maximum shearing stress condition. It suggests that in the state of yielding, the maximum shear stress at all points of a medium has the same value for a given material, equal to half the yield stress in simple tension. Von Mises' yielding condition (J_2 theory) is based on the constant shearing stress intensity condition given by

$$(\sigma_1 - \sigma_2)^2 + (\sigma_2 - \sigma_3)^2 + (\sigma_3 - \sigma_1)^2 = 2\sigma_0^2 . \quad (2.2)$$

In case of pure shear von Mises condition of constant maximum shear stress reduces to

$$\tau_0 = \frac{\sigma_0}{\sqrt{3}} . \quad (2.3)$$

This condition is in better agreement with experimental data for ductile metals than Tresca-Saint Venant condition, hence is widely used to model plastic behavior of metals. Thus, according to von Mises theory of plasticity, uniaxial stress and strain are related to stress and strain in simple shear by

$$\tau = \frac{\sigma}{\sqrt{3}} \quad (2.4)$$

$$\gamma = \sqrt{3}\varepsilon . \quad (2.5)$$

2.2 Finite Element Simulations

Specimens of various shapes have been used by investigators in high strain rate shear testing of metals. Top hat specimen, double notch shear specimen are widely used to study adiabatic shear banding in metals. Many experimental results are available in literature for different metals, but only few authors have used numerical simulations to verify the experimental data. Klepaczko (1994) performed finite element analysis of Modified Double Shear (*MDS*) Specimen. Based on the results obtained from the numerical study, a calibration factor was introduced to correct the experimental data. Chung *et al.* (1994) conducted numerical and experimental study of formation of adiabatic shear band.

Before shear stress-strain curve from the experiments can be used to construct the constitutive law for the material, it is necessary to know the state of stress in the

specimen. Different geometries used in literature for shear testing introduce considerable bending in the specimen. Also, sharp corners near the shear zone give rise to stress concentration in the specimen, which has considerable effect on its load-displacement response. The present study was undertaken to analyze the stress distribution in the specimen during the deformation and to investigate its influence on the boundary measurements of load and displacement. Following sections describe the results of numerical simulations performed on different specimen geometries. All the geometries were modeled using finite element software ABAQUS. ABAQUS is commercially available finite element software developed by Hibbitt, Karlsson & Sorensen Inc. IDEAS (finite element and solid modeling software by Structural Dynamics Research Corporation) preprocessor was used to generate axisymmetric and 2-D mesh. Six noded triangular elements were used in all simulations. Results of the finite element analysis were displayed using ABAQUS postprocessor.

2.2.1 Material Model

J_2 deformation plasticity option available in the standard library of ABAQUS was used to model the metal plasticity in the finite element simulations. This model is based on Ramberg-Osgood power law hardening. The constitutive relationship for the material is given by

$$\frac{\varepsilon}{\varepsilon_0} = \frac{\sigma}{\sigma_0} \qquad \text{for, } \sigma \le \sigma_0 \tag{2.6}$$

$$\frac{\varepsilon}{\varepsilon_0} = \frac{\sigma}{\sigma_0} + \alpha\left(\frac{\sigma}{\sigma_0}\right)^n \qquad \text{for, } \sigma > \sigma_0 \tag{2.7}$$

where α is the elastic offset, ε_0 is the elastic yield strain, σ_0 / E, σ_0 is the yield stress of the material and n is the hardening exponent. The strain can be decomposed into elastic and plastic components, $\varepsilon = \varepsilon^e + \varepsilon^p$, where $\varepsilon^e = \sigma / E$. In 1-D (uniaxial stress), σ and ε can be viewed as the axial stress and strain respectively. In 3-D, σ and ε can be viewed as the equivalent stress and equivalent strain respectively (see Section 2.1 for details).

The material used in this numerical study was 2024-T3 aluminum. This material is known to be rate insensitive for a wide range of strain rates (10^{-4} s^{-1} to 10^4 s^{-1}). Thus, numerical results obtained from the quasi-static loading condition can be used for comparison with the experimental results at different strain rates. Uniaxial stress-strain curve for this material determined by Hodowany (1997) was fitted with Ramberg-Osgood law. Values of the different parameters used are listed in Table 2.1.

Table 2.1 Selected Mechanical properties of 2024-T3 aluminum

Young's Modulus E	Yield Stress σ_0	Offset α	Hardening Exponent n
70 GPa	275 MPa	0.51	6.17

2.2.2 Axisymmetric Top Hat Specimen

2.2.2.1 Shear Stress-Strain Measurements

As mentioned earlier, top hat specimen has been used for obtaining shear stress-strain curves at high strain rates. The geometry of the specimen is illustrated in Fig. 2.1. This specimen was first used by Meyer *et al.* (1981) to study the properties of metals under localized shear. Beatty *et al.* (1991), Andrade *et al.* (1994), and Meyers *et al.*

(1995) used this specimen to analyze the shear deformation of 4340 steel. A split Hopkinson compression bar is used to load the specimen at high strain rates. The geometry of the specimen causes intense shear deformation in the ligament between the solid top hat section and the hollow cylindrical base. Average shear stress in the ligament, $\tau(t)$, is obtained by dividing the load carried by the specimen, $P(t)$, by cross-sectional area, A_s, of the ligament.

$$\tau(t)=\frac{P(t)}{A_s}, \tag{2.8}$$

where $A_s = 2\pi r_{av} l_s$, r_{av} being mean radius of the shear zone and l_s being its length.

Average shear strain in the ligament is given by

$$\gamma(t)=\frac{u(t)}{\delta} \tag{2.9}$$

where $u(t)$ is the boundary displacement imposed on the specimen and δ is the width of the ligament. Shear stress and strain obtained in this way from boundary measurements is used to construct shear stress-strain curve for the material used. This curve can be used as a constitutive law for the material only if the ligament is under simple shear. Even though the ligament undergoes high shear deformation, the state of stress in the shear zone is not that of simple shear. The bending moment causes considerable bending of the cylindrical section and sharp corners near the ligament give rise to stress concentration. The goal of this numerical study is to quantify the effect of these factors on the shear stress-strain curve obtained from the boundary measurements.

2.2.2.2 Numerical Simulation of Axisymmetric Top Hat Specimen

Based on symmetry, only one half of the axisymmetric top hat specimen (Fig. 2.1) was considered in the simulation. Six noded triangular axisymmetric elements, CAX6,

were used to model the geometry. The total number of elements used was 2294 and number of nodes was 4731. The mesh was refined in the shear zone and near the corners as shown in Fig. 2.2. The smallest element size used was 0.025 mm (25μm). The base of the specimen was constrained from moving in vertical direction and displacement boundary condition was imposed on the upper boundary. The specimen was loaded statically until the average shear strain reached a value of 0.75. At each time step, the displacement of the upper boundary, load carried by the specimen and shear stress-shear strain at the centroid of each element in the shear zone was stored.

Shear stress contours in the shear zone are plotted in Fig. 2.3. As expected, distribution of shear stress in this region is not uniform. Shear stress contours emanating from the upper and lower corner expand into the shear zone and finally merge into each other. Shear strain contours in Fig. 2.4 show that shear strain distribution in the shear zone is not uniform. Shear strain in most of the elements in this region is lower than that obtained from boundary measurement using equation (2.9). Also, there is considerable stress concentration near both the corners. This leads to plastic deformation in the supports near the corners. Distribution of the Mises stress in the specimen is shown in Fig. 2.5. It is important to see the effect of these factors on the load vs. displacement response of the structure. The uniformity of shear stress and shear strain in the shear zone can be determined by comparing their average value in the shear zone with that obtained from the boundary measurements of load and displacement, which is used in experiments to determine the constitutive response of materials (Vecchio, 1994, Minnar & Zhou, 1998).

Figure 2.6 shows the comparison of two curves obtained from different methods of measurement. Average shear stress-strain curve in this plot is the average of shear stress and shear strain values at the centroid of all elements in the shear zone. Shear stress-strain curve from the boundary measurements is obtained from the load vs. displacement curve using equations (2.8) and (2.9). The difference between the two curves is because of non-uniformity of shear stress in the shear zone. It is noticeable that the levels of shear stress in both the plots are the same, but shear strains are off almost by the factor of two. Thus, for a given displacement, shear stress obtained by dividing load by the shear area is same as average value of shear stress in the shear zone, but the strain computed from the boundary displacement is not the same as average shear strain in the shear zone. In calculating shear strain, $\gamma(t)=u(t)/\delta$, it is assumed that displacement $u(t)$ applied to the boundary of the specimen and the displacement $u_s(t)$ near the shear zone are the same. The difference between the two displacements would be small only if the top of the top hat specimen remains elastic. This concept is illustrated schematically in Fig. 2.7. The results of the numerical simulations show that there is considerable plastic deformation in both the top and the support near the corners of the shear zone. Also, the deformed specimen geometry in Fig. 2.2 shows that there is considerable bending in the shear zone. Presence of bending stresses show that the state of stress in the shear zone is not that of a simple shear. Fig. 2.8 shows the difference between the two curves for the top hat specimen. It can be seen that the yield stress for the stress-strain curve obtained from the boundary measurements is lower than that for the constitutive law, but the hardening exponent is almost the same for both the curves. Thus, it can be concluded from the numerical simulations of the axisymmetric top hat specimen that shear stress

and shear strain calculated using equations (2.8) and (2.9) do not represent simple shear behavior of the material.

It is evident from the comparison between two curves in Fig. 2.8 that if stress-strain data from boundary measurements is used as a constitutive model for the material, then shear stress will be underestimated and shear strain will be overestimated. The high values of shear strains based on the boundary measurements are partly because of plastic deformation in the cylindrical top section of the specimen. It was decided to observe the effect of length of this solid top section on the measurement of shear strain. Three top hat geometries with lengths of the solid top section equal to 0 mm, 2 mm and 4mm were simulated. All other dimensions were kept the same as before. Each time shear stress-strain curve from boundary measurements using equations (2.8) and (2.9) was obtained. All the three curves are plotted together with the constitutive law in Fig. 2.9. It can be observed that as length of the solid top section decreases, the difference between the strain obtained from the boundary measurements and the constitutive law decreases. The difference is not significant for finite length of the top section, but is noticeable for extreme case where length of the top section is 0 mm, i.e., there is no hat. This can be explained with the help of Fig. 2.7. Elastic deformation in the solid top section of the specimen decreases as its length decreases, but still there is considerable plastic deformation near the corners. When the length of the top section is 0 mm, the boundary displacement is directly given to the shear zone. Boundary displacement $u(t)$ in this case is same as $u_s(t)$, the displacement near the shear zone, and the shear strain values obtained from the boundary measurements are closer to the constitutive law than other two cases.

2.2.3 Axisymmetric H Specimen

An ideal geometry would be one for which shear stress-strain curve obtained from the boundary measurements matches with the constitutive law used in the finite element model.

In order to minimize the plastic deformation in the supports, it was decided to replace the supports in top hat specimen with the material with much higher yield stress. This led to another axisymmetric geometry called H specimen. As shown in Fig. 2.10, a punch is used to load the specimen whose cross section is like letter H. Shear zone in this case is the clearance between punch and the specimen. The number of elements used to model one half of the geometry was 1814 and total number of nodes was 3735. As in the case of axisymmetric top hat specimen, base of the specimen was constrained from moving in vertical direction and displacement boundary condition was imposed on the upper boundary of the punch. The specimen was loaded statically until the average shear strain reached a value of 0.75. Finite element simulation in this case shows that the average shear strain in the shear zone is closer to shear strain based on the boundary displacement. The yield stress from the boundary measurements is closer to the yield stress from the constitutive law and hardening exponent is almost the same for the two curves, but still they do not match exactly with each other. The results of the computations are shown in Fig. 2.11. Although numerical simulation predicts better results from this geometry, the stress concentration at the punch corners could lead to fracture of the ligament in high strain rate experiments.

2.2.4 Plane Specimen

There are other specimen geometries which can give slightly better results than the top hat and the H specimen, but most of them have drawbacks when used in high strain rate experiments. Also, average shear stress-strain from the boundary measurements never matches exactly with the constitutive law, because there is always some bending present in the shear zone. But, load-displacement data obtained from the experiments on these specimens can be used to deduce the constitutive behavior of the material using numerical simulations. The goal would be then to predict a constitutive law that will reproduce the experimental curve from the finite element simulation of the experiment itself.

The specimen geometry used in this study is similar to the top hat specimen geometry, only difference being that the new specimen is planar instead of being axisymmetric. The advantage of such a specimen is that it can be fabricated easily and temperature measurements can be made in the shear zone, which is almost impossible in the case of axisymmetric top hat specimen. Fig. 2.12 shows planar version of the axisymmetric top hat geometry. The base of the planar specimen was completely constrained from moving in the vertical direction and displacement boundary condition was imposed on the upper boundary of the specimen. Results of the numerical simulation are shown in Fig. 2.13. The results are similar to those obtained for the axisymmetric top hat specimen and the difference between the shear stress-strain curve obtained from the boundary measurements and the constitutive law can be noticed. However, an analog of axisymmetric top hat geometry in the form of plane specimen tends to bend and open up from the base during the experiments. Since bending

introduces additional stress concentration, it is necessary to restrict this bending by providing some type of constraint.

Two types of constraints were investigated in the experiments. First, one was a small rectangular piece of aluminum pinned to the base of the planar specimen to avoid bending. The second one was a U-shaped block of tool steel, which slid under the specimen restricting it from bending. Geometry of these specimens and experimental results obtained from them will be discussed in the next chapter. Addition of the constraints makes it difficult to model these specimens exactly using finite element analysis. Instead, if the constraint were built-in, then the numerical simulation of the geometry would be more realistic. The best geometry would be one that simulates this constraint closely. This leads to natural choice of the plane specimen with built-in constraint, shown in Fig. 2.14. 2102 six-noded triangular elements in plane stress, CPS6, were used to model this geometry while the total number of nodes was 4325. Boundary conditions were the same as those applied for other specimens. Shear stress-strain curve obtained from the boundary measurements is compared with the constitutive law used and the boundary measurements curve for the axisymmetric top hat specimen in Fig. 2.15. The load-displacement response of the plane specimen is similar to that of axisymmetric top hat specimen. Distribution of shear stress, shear strain and Mises stress is shown in Fig. 2.16, Fig. 2.17 and Fig. 2.18 respectively. As expected, shear stress-strain curve from the boundary measurements for this specimen does not match with the constitutive law, the former one starting nonlinearity at much lower stress than the latter one with almost the same hardening exponent. But, the planar geometry of this specimen makes temperature measurements possible in experiments. Also, since the specimen is

made from one piece of material, it is easier to model this specimen using finite elements as compared to other plane geometries with external constraints.

2.2.5 Optimization of Specimen Geometry

The effect of aspect ratio of the shear zone on the nature of shear stress-strain curve from boundary measurements was studied by modeling three planar specimens with different aspect ratios. Aspect ratio here is the ratio of length of the shear zone to the width of the shear zone. Three aspect ratios used in this numerical study were 1,5 and 10. In each case width of the shear zone was 0.4 mm and length of the shear zone was 0.4 mm, 2.0 mm and 4 mm respectively. All other dimensions of the specimen were the same. Each time analysis was carried out until the average shear strain in the shear zone was about 0.7. Shear stress-strain curves from the boundary measurements are plotted in Fig. 2.19. It can be seen that as the aspect ratio increases from 2 to 5, shear stress is higher at higher strains. However, difference between the shear strains increases as the aspect ratio is increased. As length of the shear zone increases for fixed shear zone width, relative magnitude of the bending stresses in the shear zone decreases and the state of stress in the shear zone approaches the state of simple shear. But as the load carrying capacity of the ligament increases, the plastic deformation in the supports and bending of the arms of the specimen increases thus making difference between the shear strains larger. This can be clearly observed from comparison between the stress-strain curve obtained from the boundary measurements and the constitutive law for aspect ratio of 10 (Fig. 2.19).

The aspect ratio used in the experimental study was 5. Length of the shear zone was 1.15 mm and width was 0.225 mm. Thickness of the specimen was 8 mm. The load

carrying capacity of the specimen depends on the thickness of the specimen. In order to get detectable signal in the output bar of the Kolsky bar, the thickness should be maximum. The thickness of the specimen is limited by the diameter of the Kolsky bar.

2.2.6 Parametric Analysis

Numerical study of the plane specimen with built-in constraint (Fig. 2.14) for different constitutive laws was carried out to explore the possible relationship between various parameters of Ramberg-Osgood law. Response of the same structure for different constitutive laws is plotted on the same plot as shown in Fig. 2.20. All the five constitutive models had the same hardening exponent and Young's modulus. Only yield stress was increased from 225 MPa to 425 MPa in steps of 50 MPa. Shear stress-strain curves obtained from the simulations were fitted to Ramberg-Osgood law. Values of parameters like yield stress, elastic offset, hardening exponent and elastic slope was compared with the corresponding values for the constitutive law. The yield stress for the two curves for all the five cases is plotted in Fig. 2.21. The ratio was found to be around 1.3. Hardening exponent for both the cases, i.e., the constitutive law and the load-displacement response, was almost the same. This shows that there is some kind of numerical relationship between the two curves, and it can be used as a starting point to predict the correct constitutive behavior of the metal.

Planar specimen with built-in constraint was found to be optimal for this study. Same is true for the axisymmetric top hat specimen. In the case of planar specimen, it is possible to fabricate such a specimen, which will be discussed in the following chapter. In case of axisymmetric top hat specimen, it is not possible to completely restrain the specimen in a natural way.

Quasi-static and high strain rate tests were conducted on the specimen geometries discussed in this chapter. Chapter 3 will discuss how finite element results from this study are used with experimental results to predict pure shear behavior of the material.

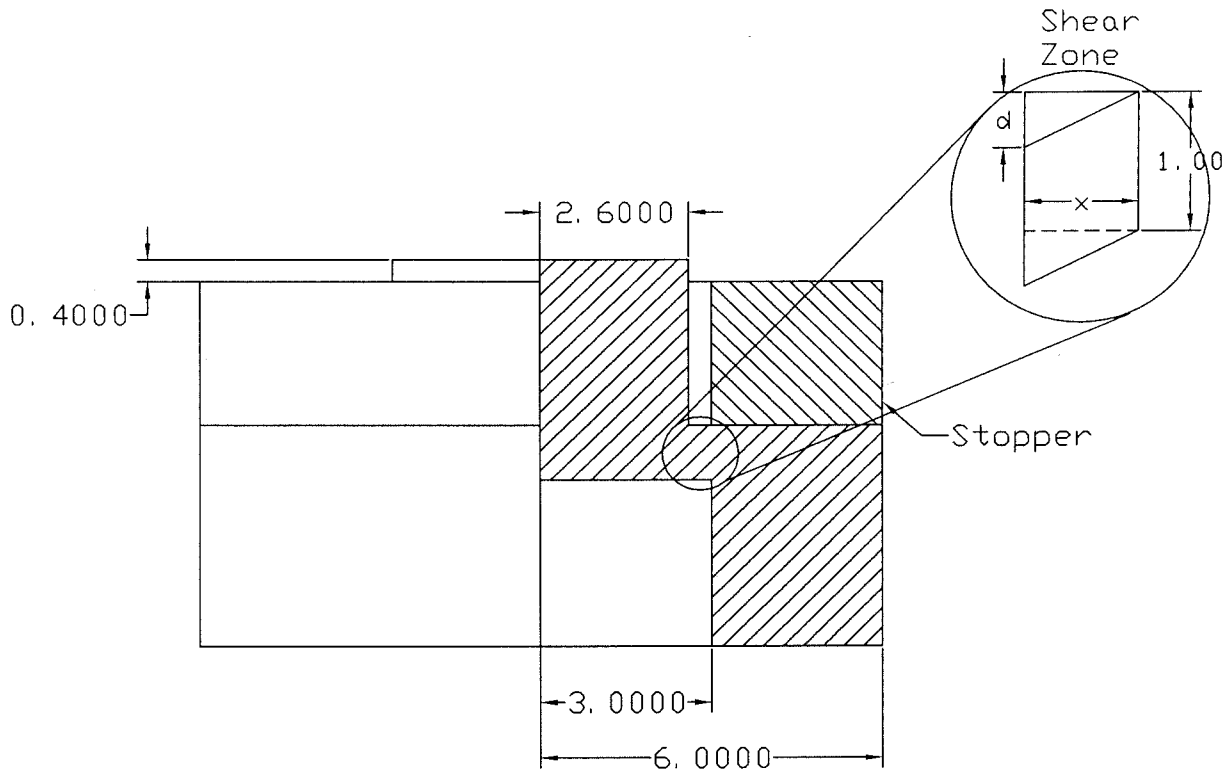

Figure 2.1 Axisymmetric top hat specimen

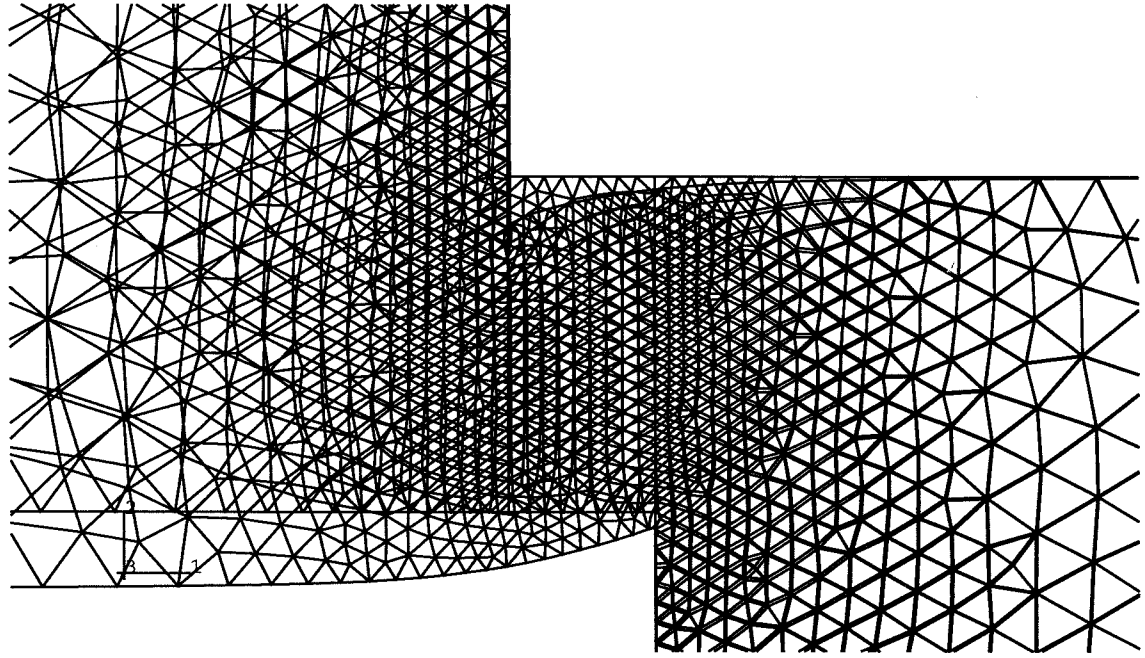

Figure 2.2 Undeformed and deformed mesh (top hat specimen)

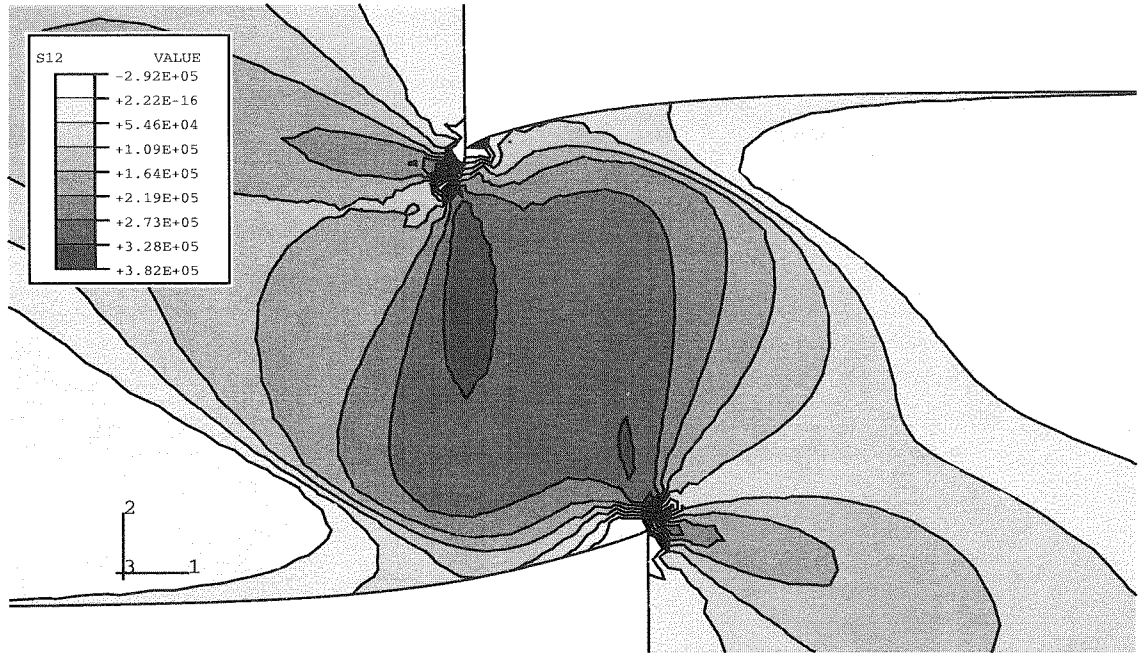

Figure 2.3 Shear stress contours (top hat specimen)

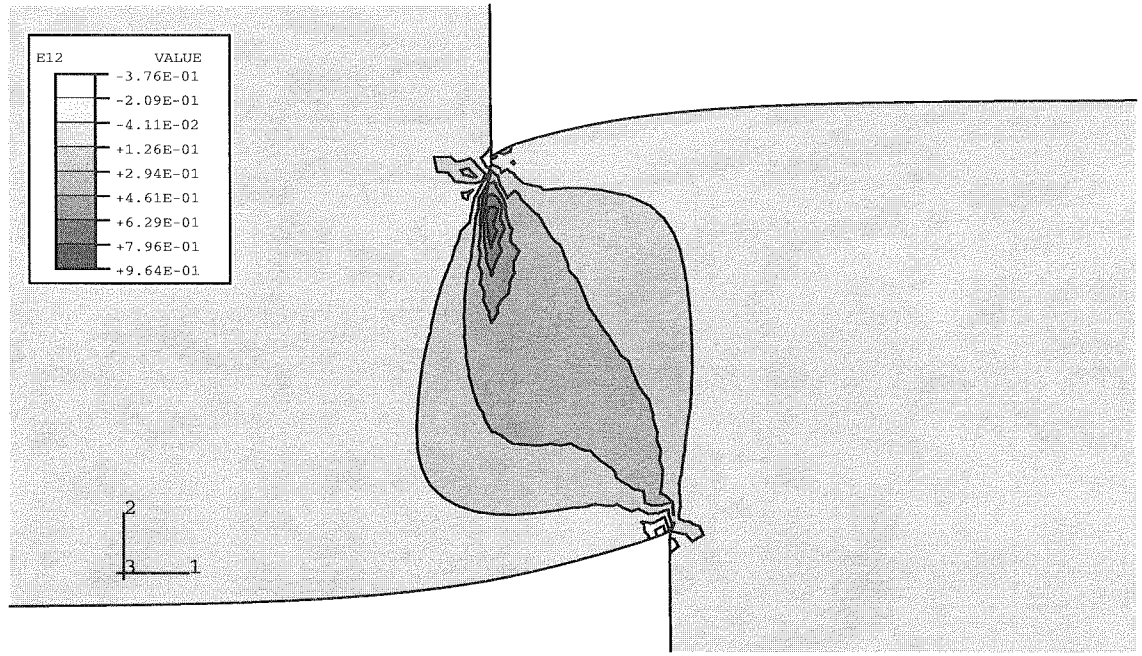

Figure 2.4 Shear strain contours (top hat specimen)

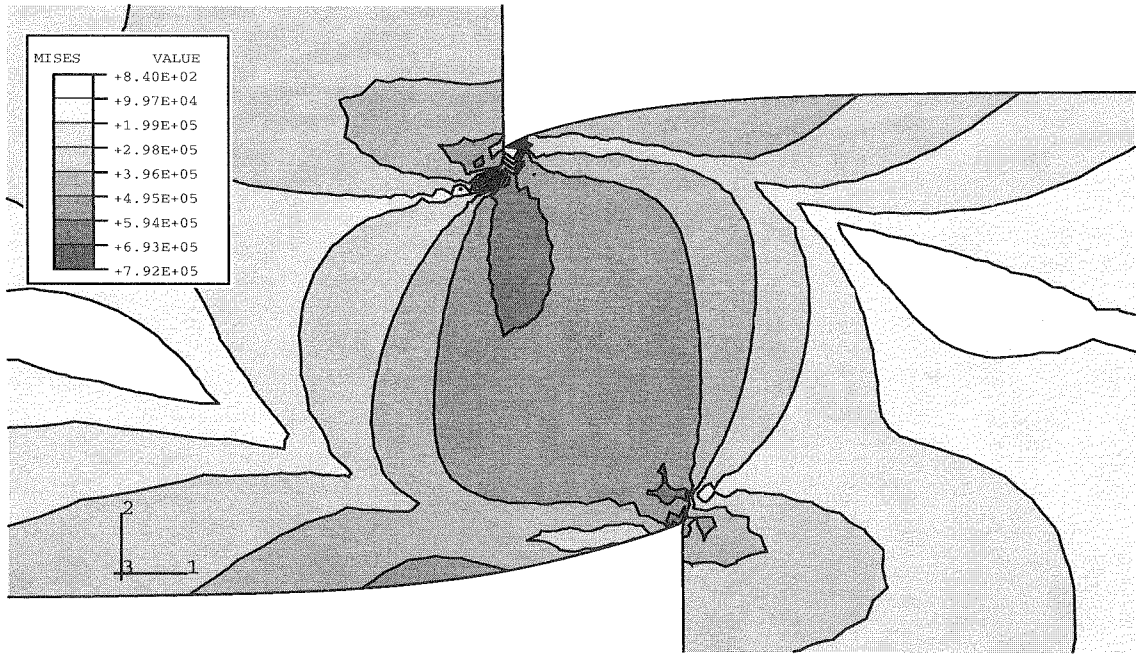

Figure 2.5 Mises stress contours (top hat specimen)

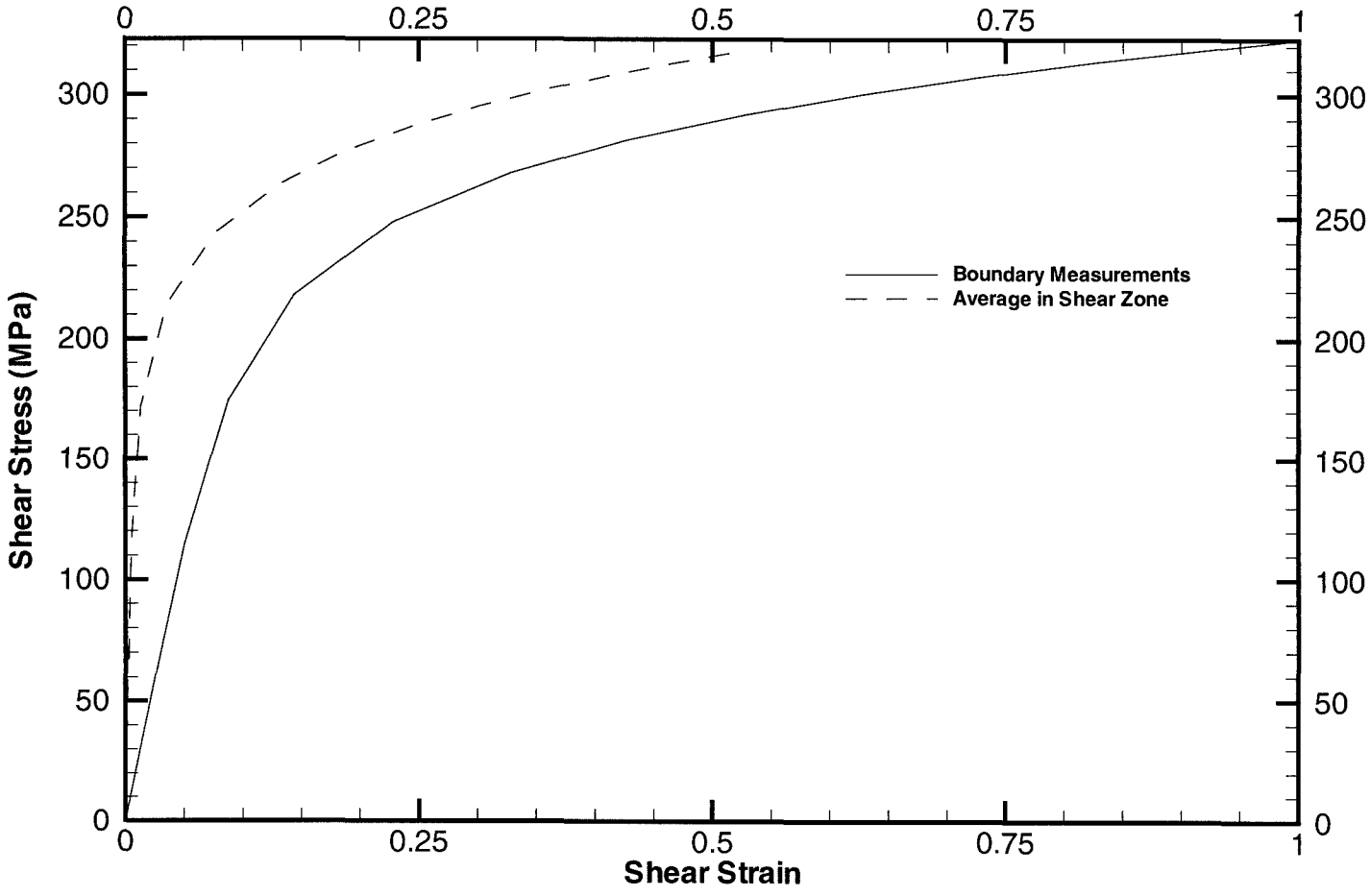

Figure 2.6 Comparison of average shear stress-strain curve in shear zone with that obtained from boundary measurements (top hat speciemen)

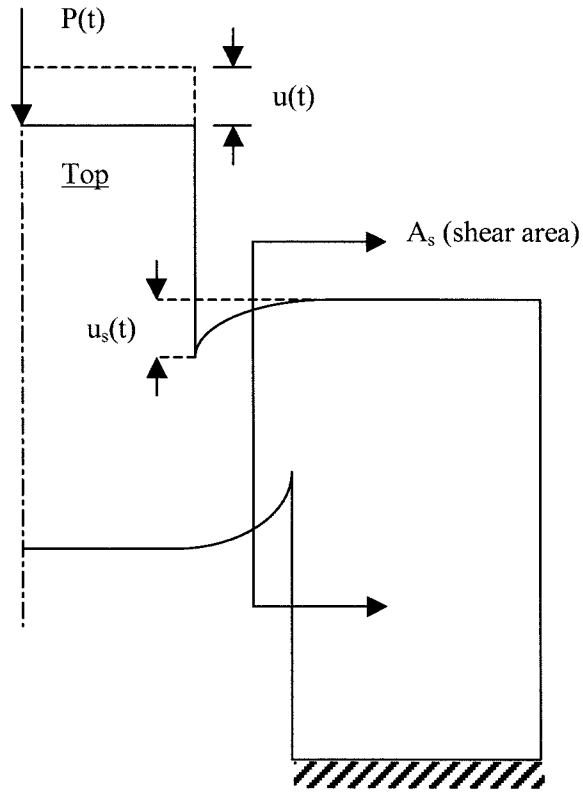

$u(t) \sim u_s(t) \Rightarrow$ Top elasic
$u(t) >> u_s(t) \Rightarrow$ Top plastic

Figure 2.7 Schematic showing measurement of shear strain

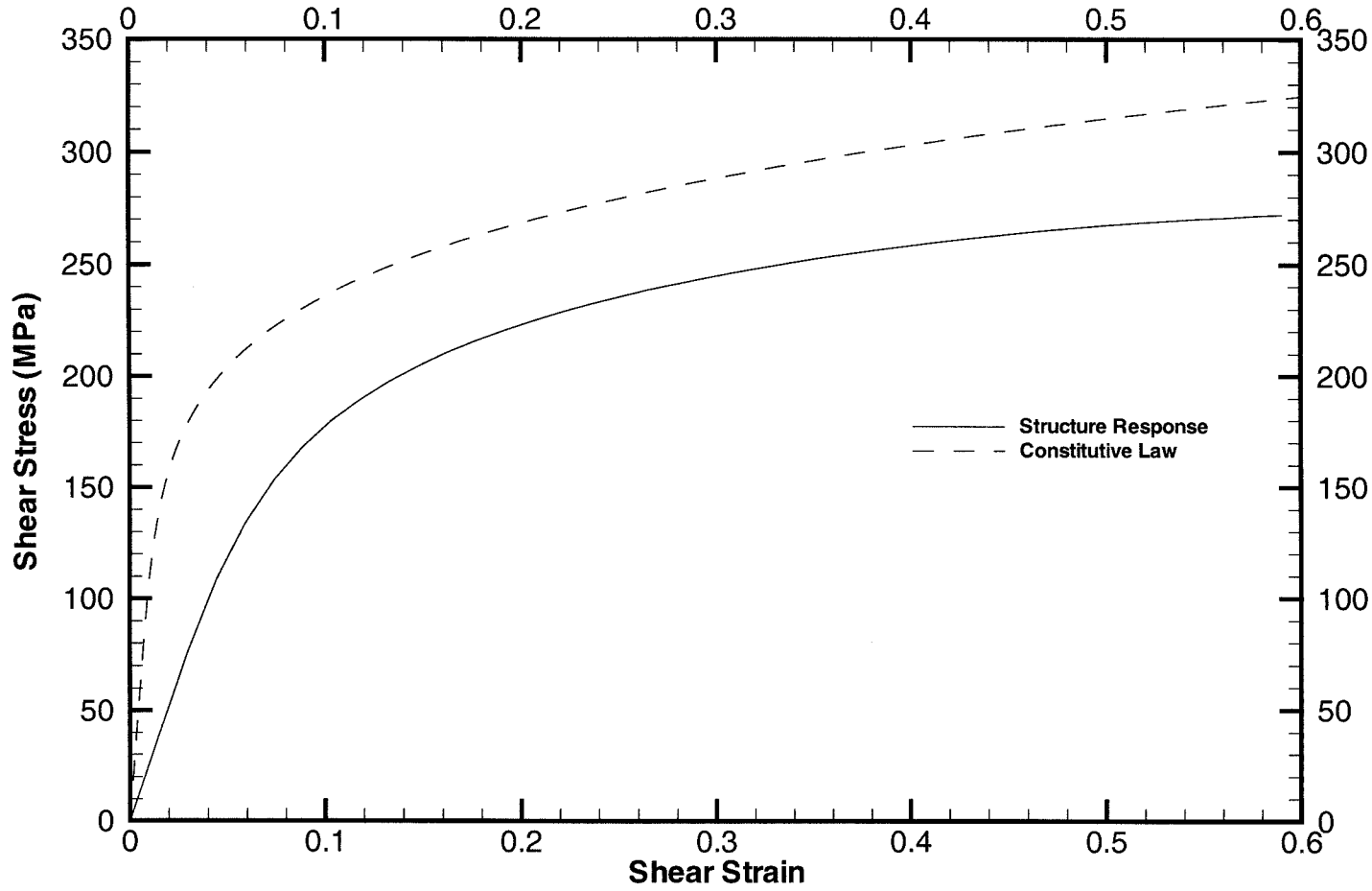

Figure 2.8 Comparison between the constitutive law and boundary measurements for top hat specimen

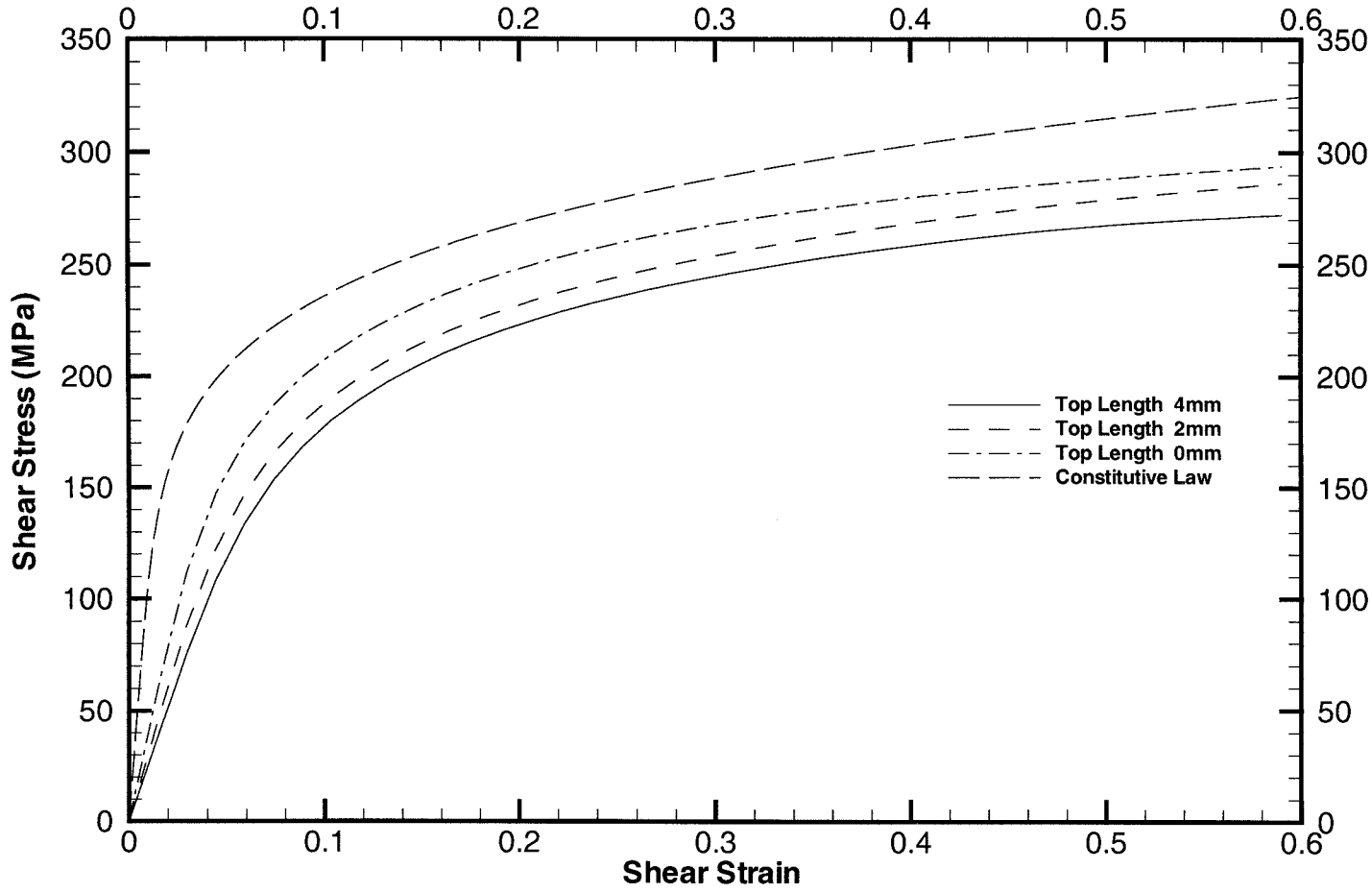

Figure 2.9 Boundary measurements of shear stress-strain for different lengths of solid top section for top hat specimen

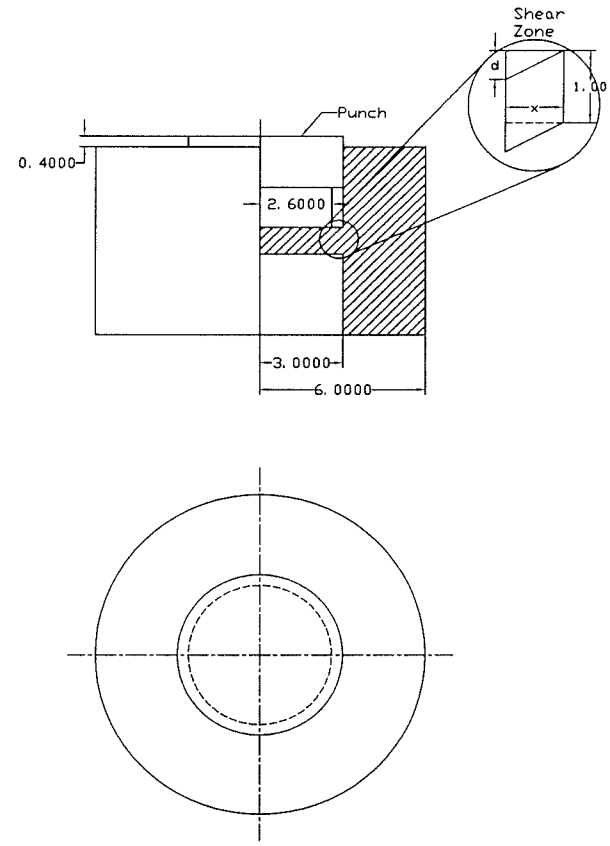

Figure 2.10 Axisymmetric H specimen

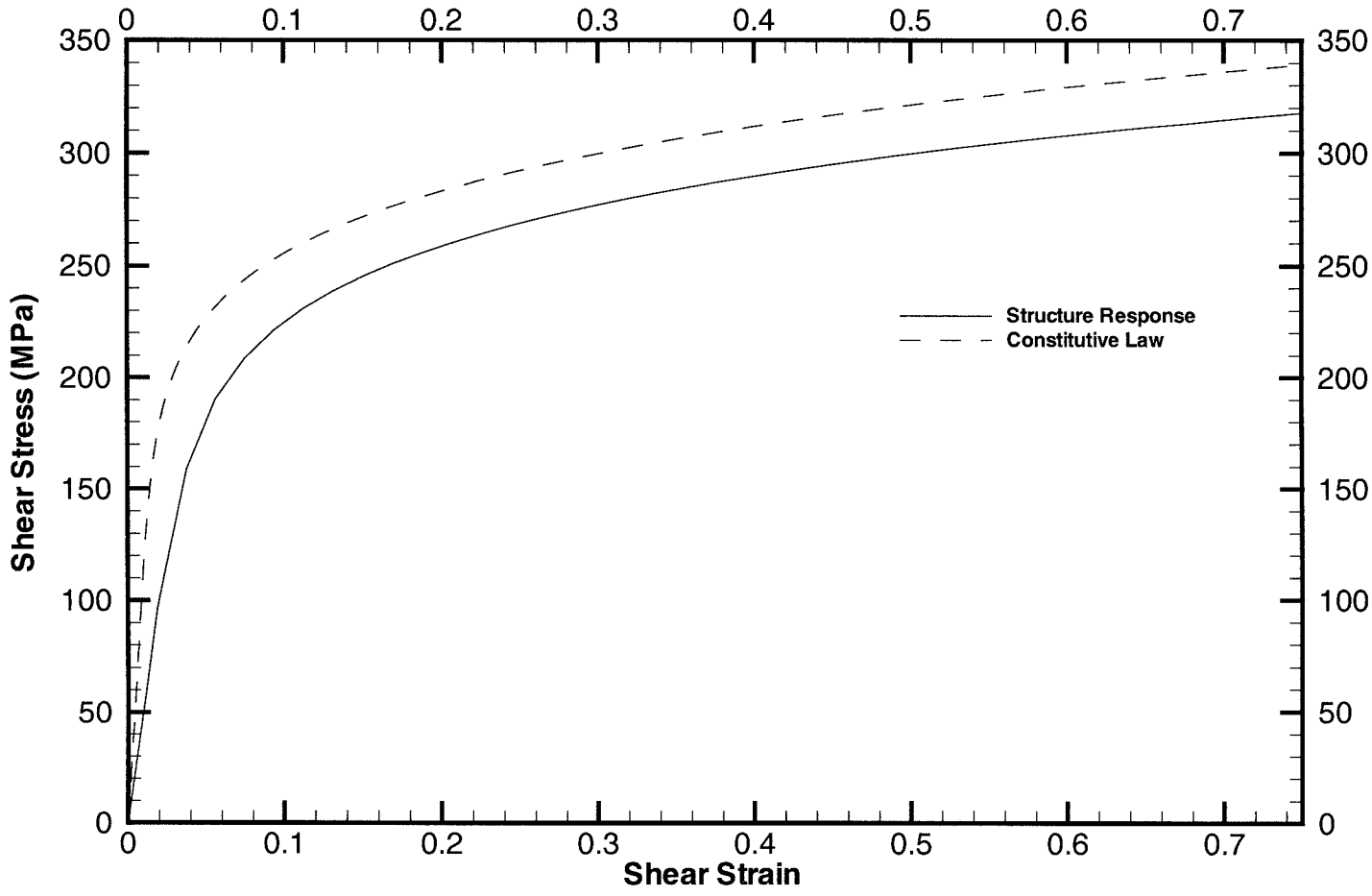

Figure 2.11 Comparison between the constitutive law and boundary measurements for axisymmetric H specimen

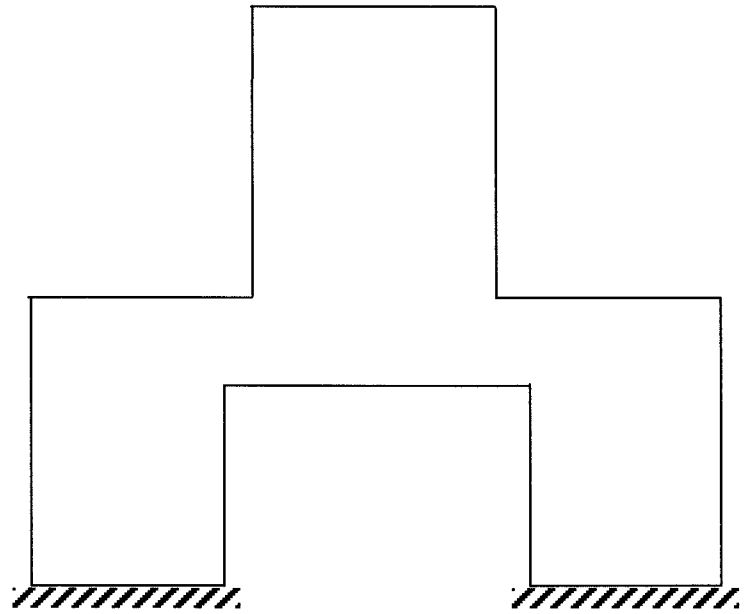

Figure 2.12 Schematic of planar top hat specimen without constraints

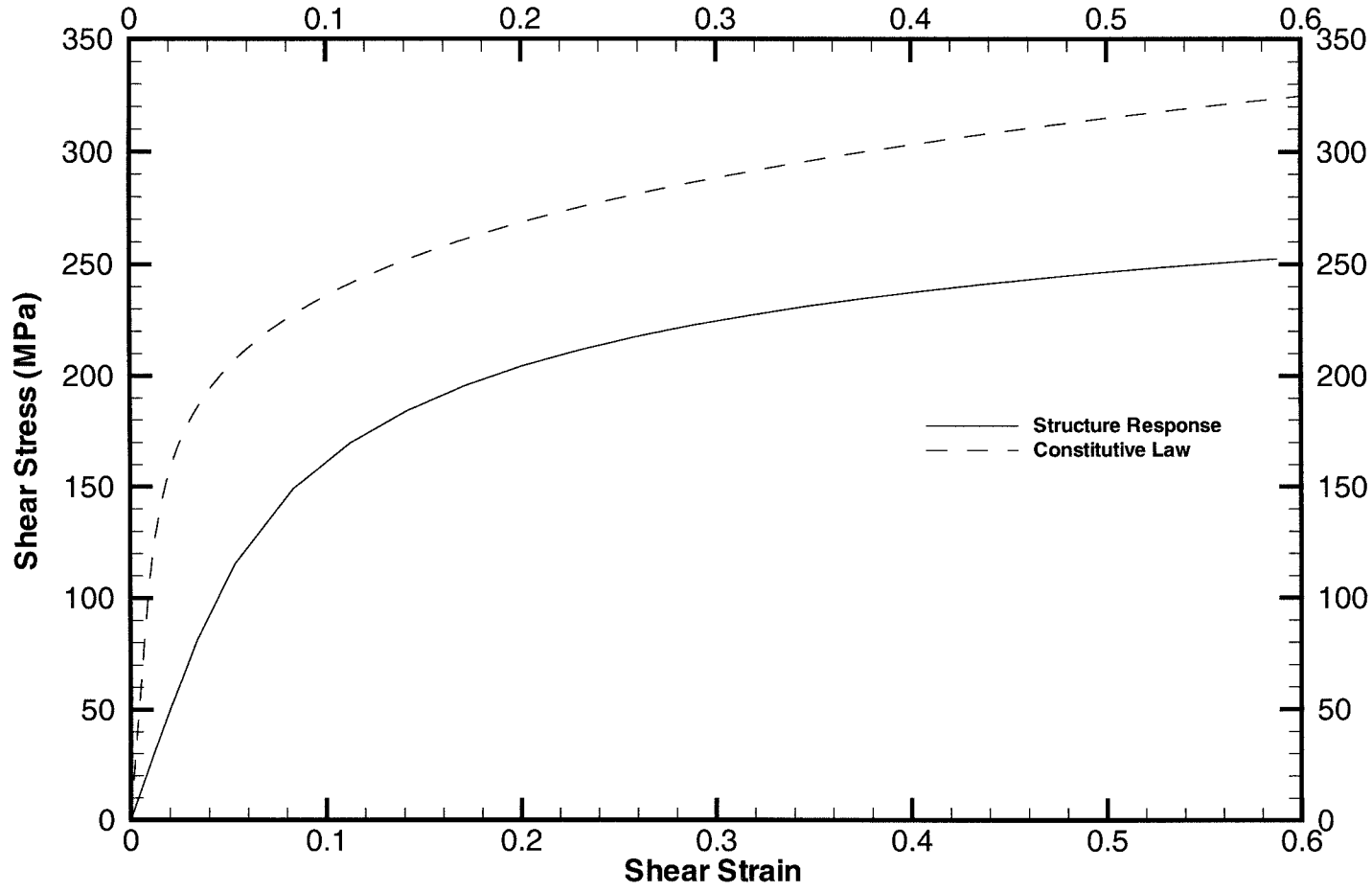

Figure 2.13 Comparison between the constitutive law and boundary measurements for planar top hat specimen

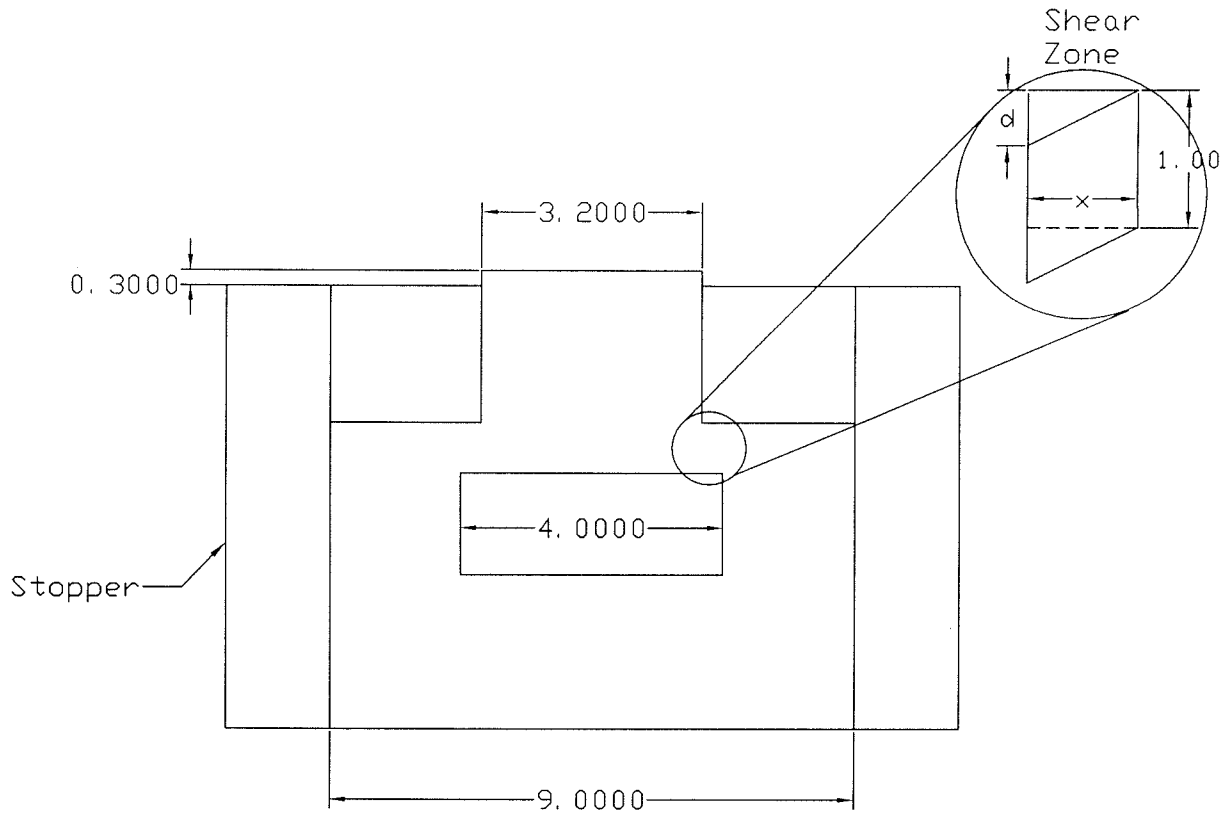

Figure 2.14 Plane specimen with built-in constraint

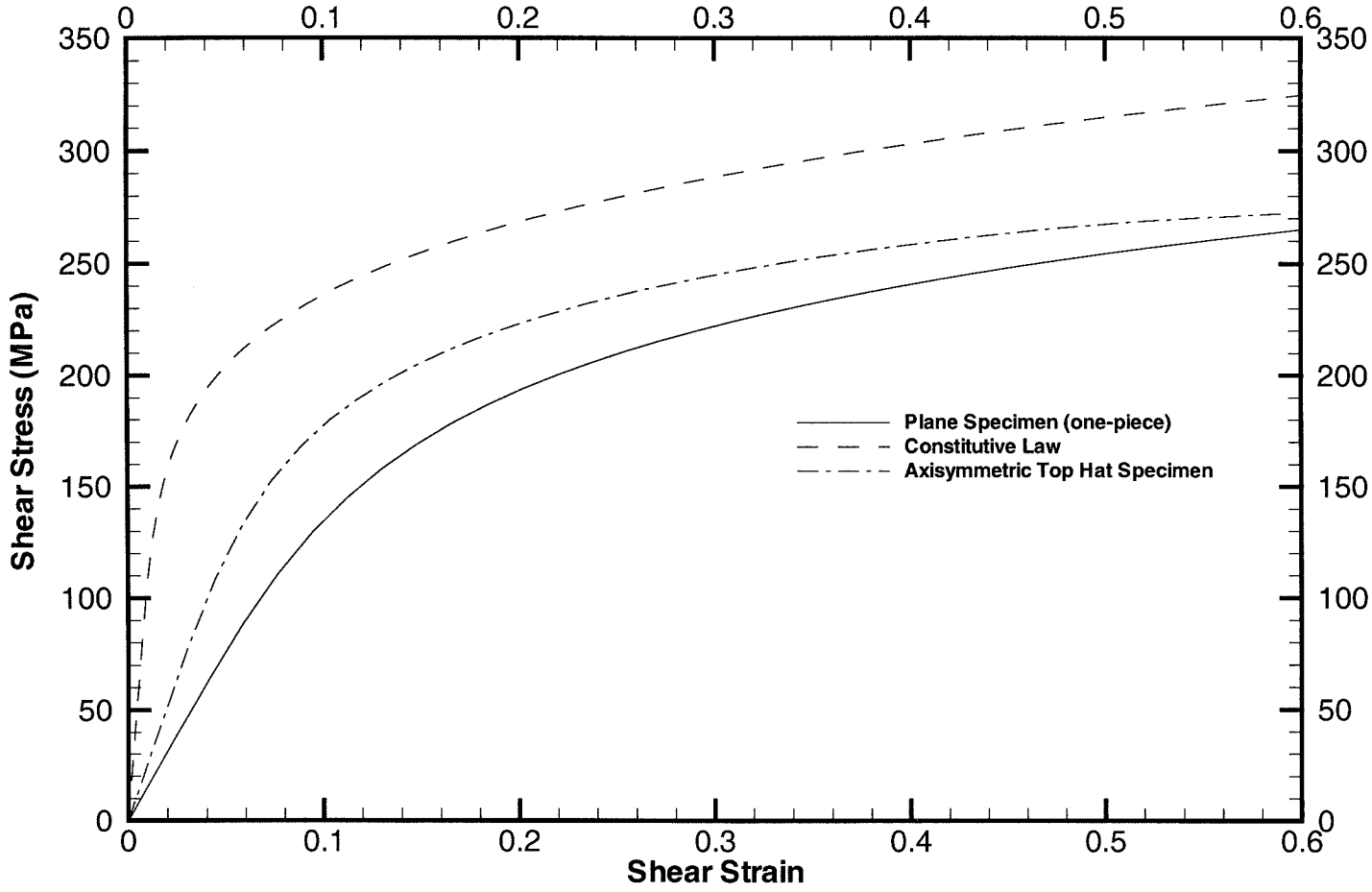

Figure 2.15 Comparison between the constitutive law and boundary measurements for plane specimen with built-in constraint and axisymmetric top hat specimen

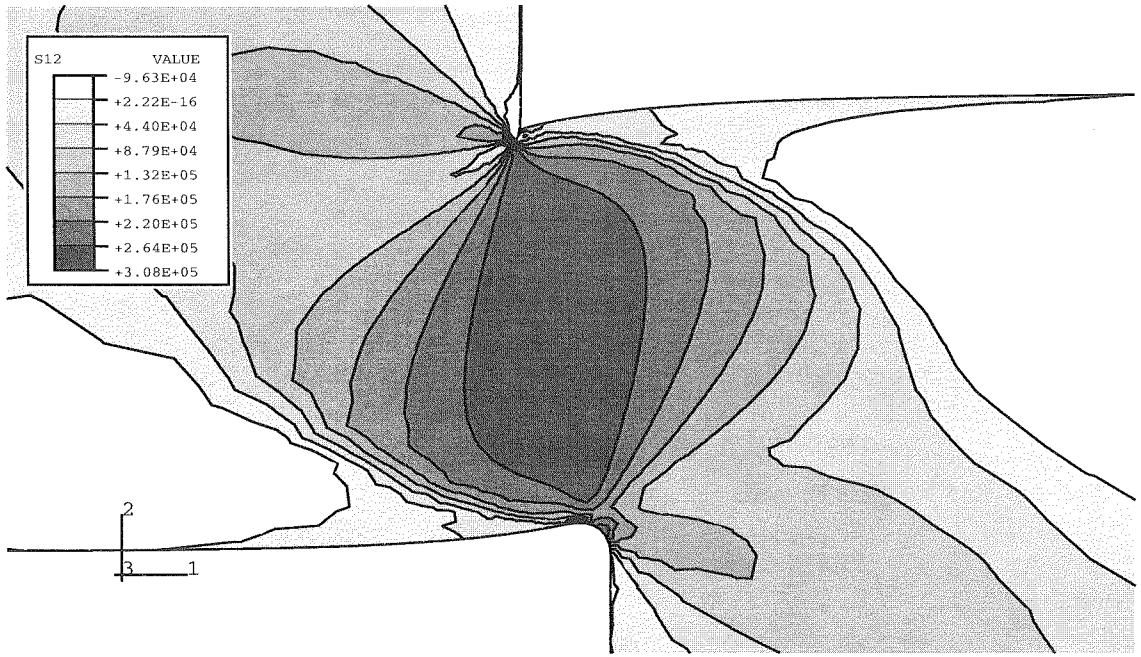

Figure 2.16 Shear stress contours (plane specimen with built-in constraint)

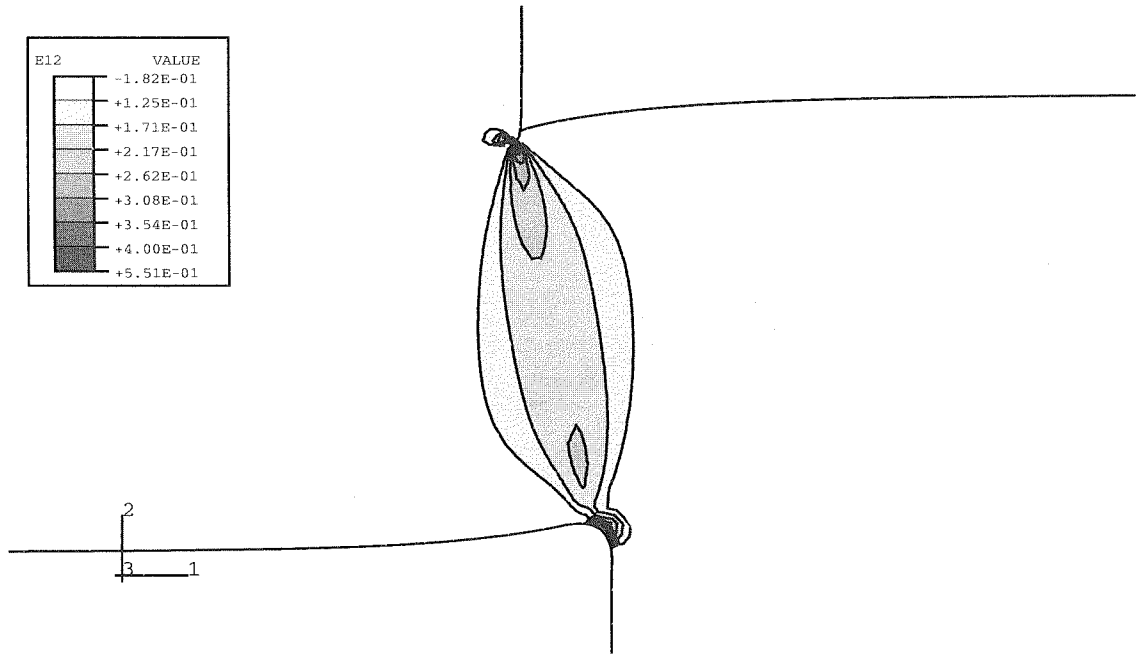

Figure 2.17 Shear strain contours (plane specimen with built-in constraint)

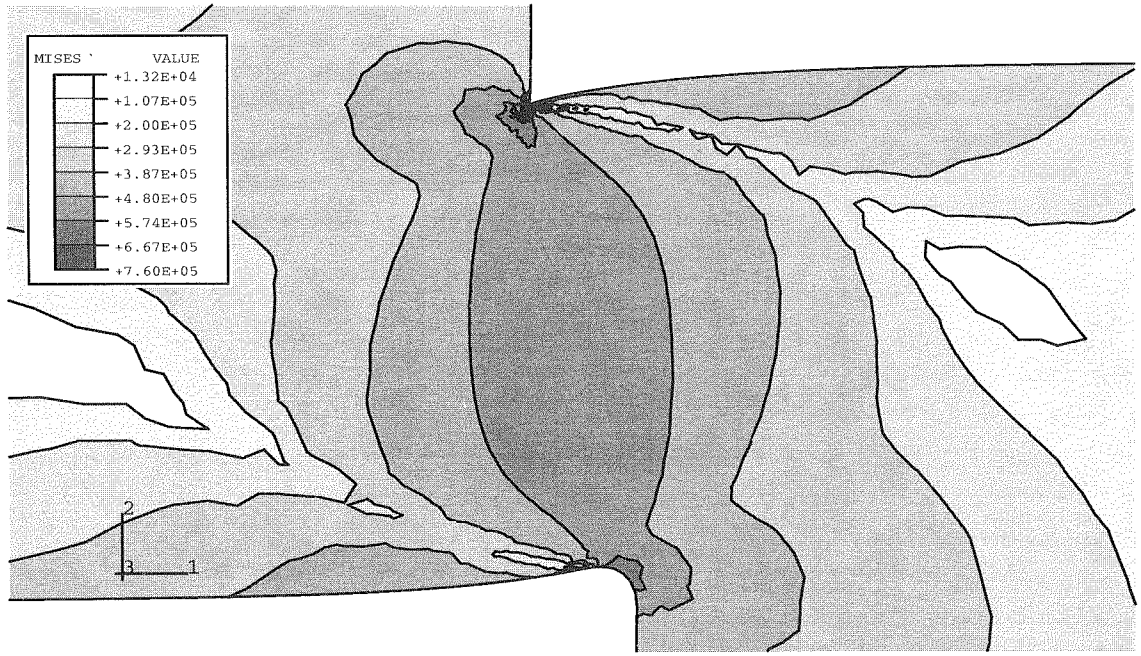

Figure 2.18 Mises stress contours (plane specimen with built-in constraint)

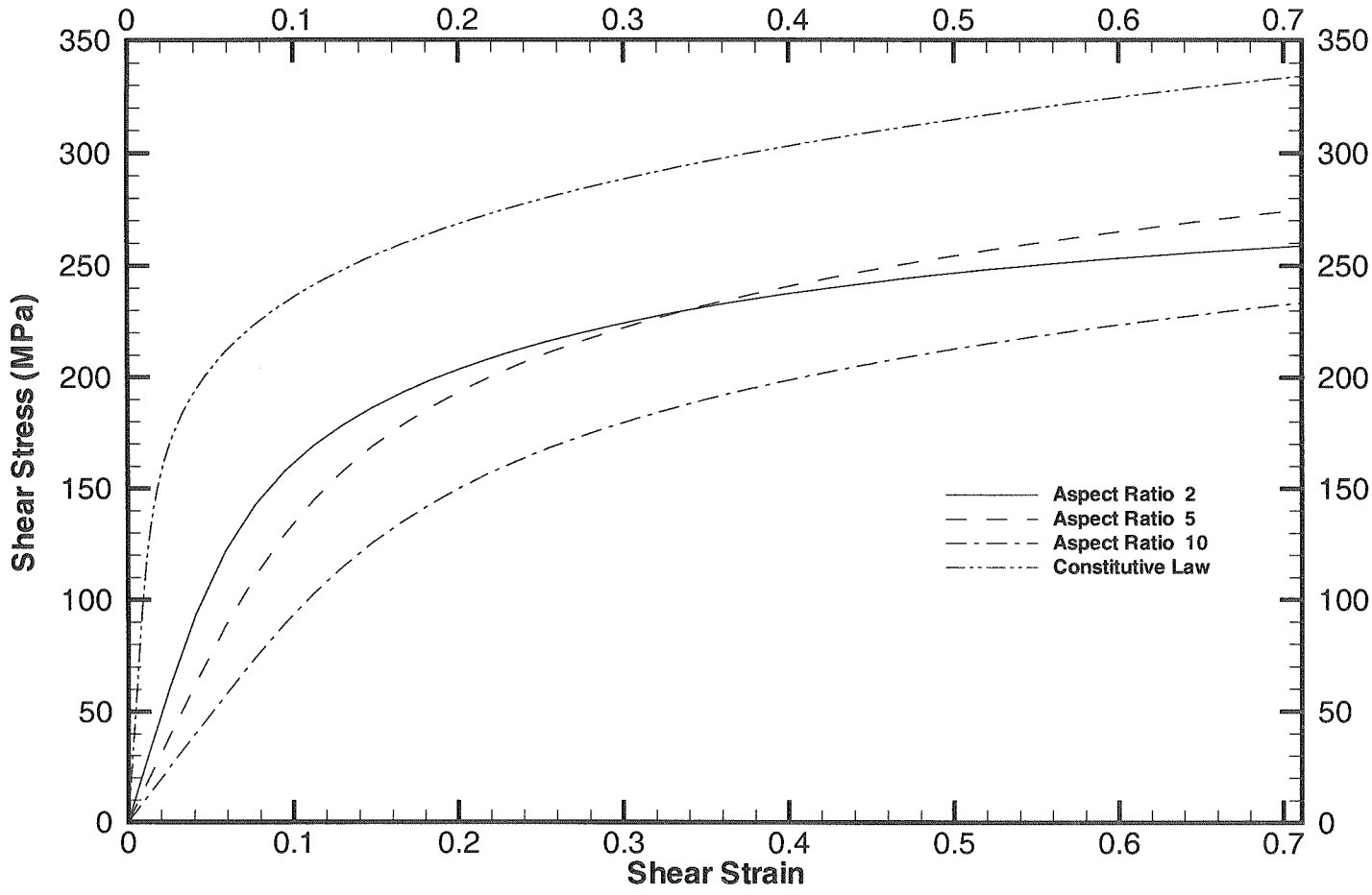

Figure 2.19 Shear stress-strain curve based on boundary measurements for plane specimen for different aspect ratios of shear zone

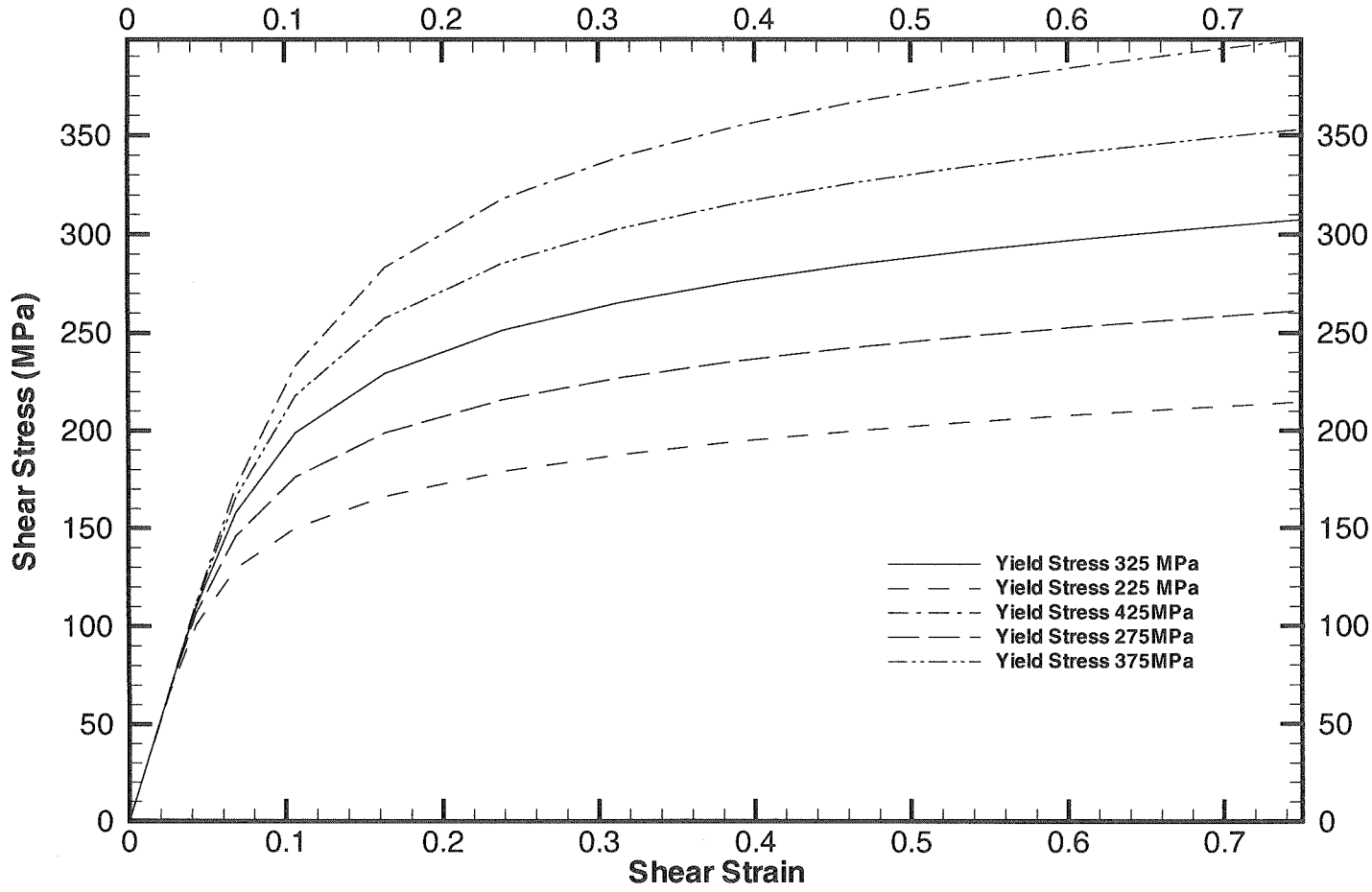

Figure 2.20 Comparison of shear stress-strain curve based on boundary measurements for five different constitutive laws

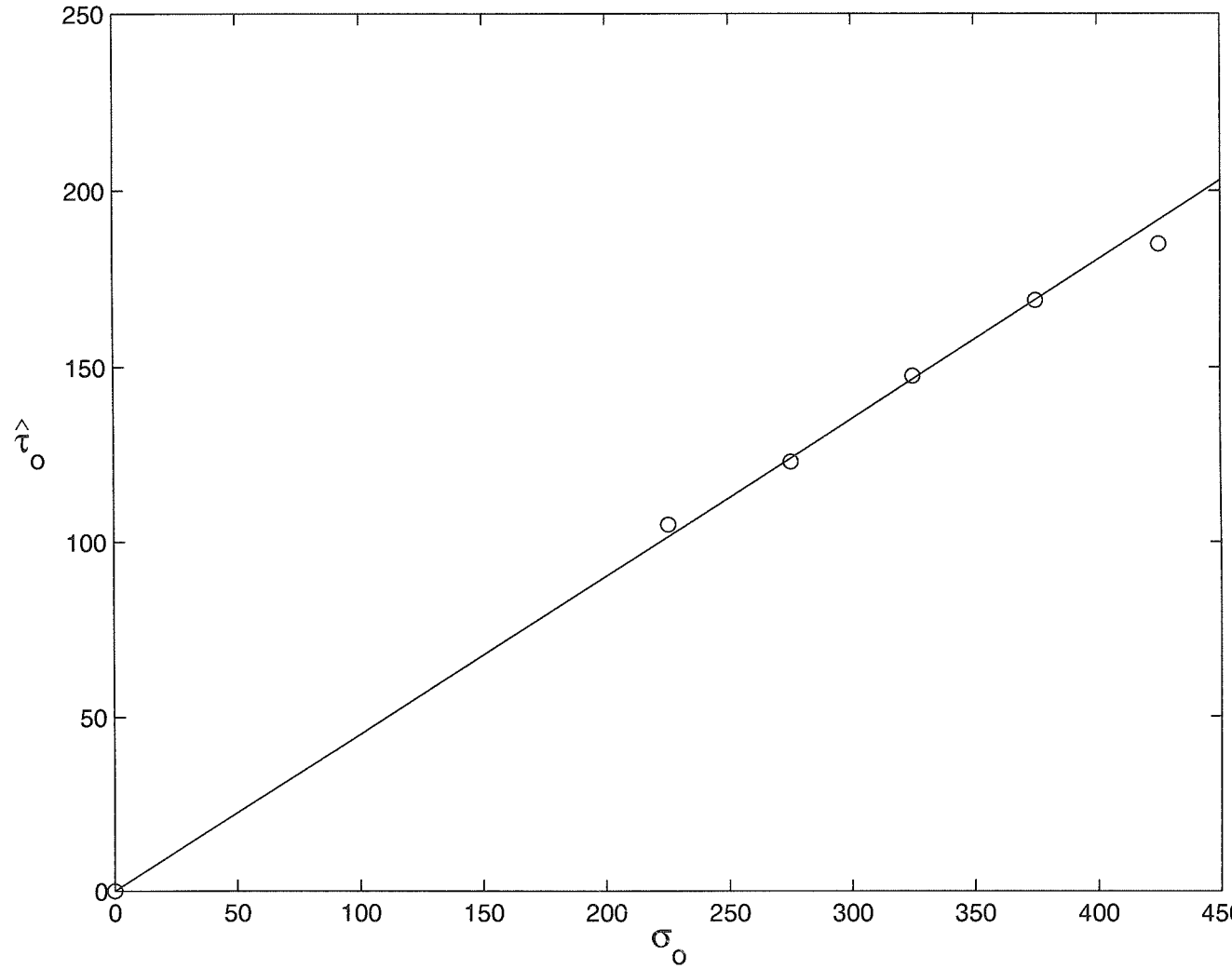

Figure 2.21 Plot of yield stress from constitutive law vs. yield stress from the fitted curve for boundary measurements

Chapter 3

Experiments

3.1 Experimental Techniques

Experiments were performed on several top hat specimen geometries using Material Test System (MTS) for low strain rates and the Kolsky compression bar at high strain rates. Following sections give brief description of the experimental setup used to carry out these experiments.

3.1.1 MTS Test Apparatus

An MTS machine (Material Test System, MTS Corporation, Minneapolis, Minnesota) was used for axial compressive loading at strain rates below 1 s^{-1}. A photograph of the apparatus is shown in Fig. 3.1 (MTS machine). An alignment fixture shown in Fig. 3.2 (alignment fixture) was used to ensure pure, one-dimensional loading. Displacement was controlled during all the experiments and load and displacement output from the transducers was recorded using data acquisition software LABVIEW. Load transducer was located in the upper arm of the machine. Stress in the specimen was calculated by dividing the load carried by the specimen by cross-sectional area of the specimen. Strain was calculated from the output of the built-in displacement transducer. Since the displacement transducer was located at the bottom of the lower loading arm, the output was corrected for the compliance of the load frame and alignment fixture.

3.1.2 Review of the Kolsky Bar in Compression

The Kolsky (split Hopkinson) pressure bar is a well-established apparatus for the high strain rate testing of ductile metals. Details of this experimental technique can be found in Lindholm (1964) and Follansbee (1985). A brief review of the technique is given below. The apparatus consists of a striker bar, an input bar and output bar as shown in Fig. 3.3, all of which are assumed to remain elastic during a test. The specimen to be tested is placed between input and output bars. When the striker bar impacts the input bar, an elastic stress pulse propagates along the length of the input bar with the longitudinal bar wave speed,

$$c_0 = \sqrt{\frac{E}{\rho}} \tag{3.1}$$

where E is the Young's modulus and ρ is the density of the bar material. The duration of the pulse is

$$t_0 = \frac{2L_{striker}}{c_0} \tag{3.2}$$

where $L_{striker}$ is the length of the striker bar. When this stress pulse reaches the specimen, a fraction of it is reflected back into the input bar and the remaining fraction transmitted through the sample into the output bar. The relative fraction depends on differences in mechanical impedance between the input bar and sample. The magnitude of the pulse in the input bar and output bar is recorded by the strain gages mounted on each bar. From one-dimensional calculations (Kolsky, 1949), the velocity gradient across the specimen can be written as

$$\frac{\partial v}{\partial x} = v' \cong -\frac{2c_0}{L}\varepsilon_R(t) \tag{3.3}$$

where v, $\left(\frac{\partial u}{\partial t}\right)$, is the particle velocity in the specimen, $\varepsilon_R(t)$ is the reflected strain in the bar and L is the length of the specimen. The relative displacement across the sample, u, can be calculated using equation (3.3) by approximating

$$\Delta v \cong v' L$$

$$u(t) = -2c_0 \int_0^t \varepsilon_R(\tau)\, d\tau \tag{3.4}$$

Hence the shear strain, γ, in the specimen can be written as

$$\gamma = \frac{u}{\delta} \tag{3.5}$$

where δ is the width of the shearing ligament. Instantaneous shear strain rate can be obtained by,

$$\frac{d\gamma}{dt} = \frac{-2c_0}{\delta}\varepsilon_R(t). \tag{3.6}$$

If the strain rate does not vary much during the experiment and is almost constant, then the average shear strain rate is given by

$$\dot{\gamma} = \frac{\gamma(t)}{t}. \tag{3.7}$$

The shearing force carried by the specimen can be calculated using the force in the transmitted bar,

$$F = A_0 E \varepsilon_T(t), \tag{3.8}$$

where $\varepsilon_T(t)$ is the strain in the output bar of cross-sectional area A_0. The stress, τ, can be calculated using

$$\tau = \frac{F}{A_s} = \frac{A_0}{A_s} E \varepsilon_T(t) \tag{3.9}$$

where the shearing area of the ligament is $A_s = 2\pi r_{av} l_s$ and $A_s = 2 l_s t$ for axisymmetric and plane geometries respectively. l_s in this case is the length of the shearing ligament, r_{av} is the mean radius of the shear zone for axisymmetric specimen and t is the thickness of the plane specimen. All the above calculations are based on the assumption that the specimen undergoes homogeneous deformation and the bars remain linearly elastic. Also, the incident and transmission bars are assumed to be of the same material and of identical and uniform cross-sectional area.

The experiments were conducted in the Kolsky bar (also called the split Hopkinson pressure bar) facility in the Graduate Aeronautical Laboratories at Caltech. The setup consists of a striker bar, an incident bar, a transmission bar and a light gas gun for propelling the striker bar. The lengths of the incident bar and transmission bar are 1220 and 580 mm respectively, with a common diameter of 12.7 mm. All the bars are made of high strength VascoMax C-350 maraging steel (Rc=57.8). The uniaxial compressive yield strength of the bars is approximately 2.7 GPa.

3.1.3 Photo-resist Grid Technique

To observe the magnitude of bending in the shear zone, a grid of photoresist was deposited on the plane specimen with pinned constraint (Fig3.11). One surface of the specimen was polished first using 1000 grit polish paper. A thin layer of Kodak KPR photoresist was deposited on this surface and was preheated to 80^0 C for 10 minutes. A moire cross grating with 1000 lines per inch was used as a mask. The photoresist was then exposed to UV light for 3 minutes and then etched in a Kodak photoresist developer. The photoresist remaining on the surface was baked at 120^0 C for 10 minutes and then immersed in a blue dye. The specimen surface was then washed with water to remove

the excessive dye sticking to the specimen surface. The shear region was photographed before and after the experiment using Nikon (Nikon Measurescope MM-22) optical microscope.

3.2 Material

All the specimens used in the experiments were made out of commercially available 2024-T3 aluminum. Since 2024-T3 aluminum is known to be rate insensitive over a wide range of strain rates, 10^{-4} s^{-1} to 10^{4} s^{-1} (Hodowany, 1997), results from the experiments conducted at different strain rates can be compared with the finite element simulations of the experiment under static loading. Ramberg-Osgood power law hardening was used to fit the uniaxial stress-strain curve for this material determined by Hodowany (1997). Values of the different parameters used are listed in Table 3.1.

Table 3.1 Selected Mechanical properties of 2024-T3 aluminum

Young's Modulus E	Yield Stress σ_0	Offset α	Hardening Exponent n
70 GPa	275 MPa	0.51	6.17

3.3 Specimen Geometries

3.3.1 Axisymmetric Top Hat Specimen

Engineering drawing of the top hat specimen used in the experiments is shown in Fig. 3.4. Length (l_s) of the shear zone is 1 mm and its width (δ) is 0.4 mm. Shear zone in this case is a cylindrical ring sandwiched between solid top section and hollow

cylindrical base. Cross-sectional area (A_s) used to calculate shear stress was based on the average radius of the shear zone, given by

$$A_s = 2\pi r_{av} l_s . \qquad (3.6)$$

r_{av}, the mean radius of the shear zone in this case, is 2.8 mm, and length of the shear zone l_s is 1 mm. A stopper ring was used to control the displacement applied to the solid top of the specimen.

3.3.2 Axisymmetric H Specimen

As discussed in the last chapter, results of numerical simulations for H specimen were better in comparison with the results for the top hat specimen. Dimensions of the geometry used in experiments are shown in Fig. 3.5. Again, length and width of the shear zone are 1 mm (l_s) and 0.4 mm (δ) respectively. Mean radius of the shear zone, r_{av}, is 2.8 mm. The punch is made from tool steel. The shearing portion of the punch has radius 2.6 mm. Cylindrical portion of the ligament between the punch and the specimen undergoes shear deformation in this case. Calculations of shear stress and shear strain are identical for the H specimen and axisymmetric top hat specimen.

3.3.3 Pinned Planar Specimen

Planar version of axisymmetric top hat specimen undergoes considerable bending if its base is not constrained. Fig. 3.6 shows a small block of aluminum pinned to the base of the plane specimen. Shear zone is 0.4 mm (δ) in width and 1 mm (l_s) in length and is planar. The thickness (t) of the specimen is 6 mm, hence the cross-sectional area ($A_s=2l_st$) used for calculation of shear stress in this case is 12 mm^2. A stopper made out of tool-steel is used to control the displacement given to the specimen. Thus, specimen

can be recovered after it undergoes shearing and can be studied to observe the nature of deformation in the shear zone.

3.3.4 Plane Specimen with Lateral Constraint

Another type of constraint used to restrict bending of the arms of the plane specimen was a U-shaped block of tool-steel. Assembly of this constraint and the specimen is shown in Fig. 3.7. Dimensions of the plane specimen are exactly, same as those for the plane specimen with pinned constraint. Arms of the U block also serve as a stopper to control the deformation in the specimen at required stage.

3.3.5 Integral, One-piece Planar Specimen

Fig. 3.8 shows the planar specimen with built-in constraint. This specimen was made in a single block using wire Electro-Discharge Machine (EDM). The shear zone is 0.225 mm (δ) in width and 1.15 mm (l_s) in length. The thickness of the specimen is 8 mm, hence the cross-sectional area (A_s) used for calculation of shear stress in this case is 18.4 mm^2.

3.4 Experimental Results

3.4.1 Axisymmetric Top Hat Specimen

Experiments were conducted on a MTS machine at low strain rates to validate results obtained from numerical simulation of the axisymmetric top hat specimen (Fig. 3.4). The tests were carried out at shear strain rate 10^{-2} s^{-1}. Fig. 3.9 shows the average shear stress-strain curve for the top hat specimen obtained from the boundary measurements of load and displacement. The shear stress was obtained by dividing load

by shear area of the specimen using equation (2.5) and shear strain was calculated by dividing boundary displacement by gage length of the shear zone using equation (2.6). The experimental curve was compared with the curve obtained from finite element simulation of the same specimen geometry. Both experimental and computed curves are plotted in Fig. 3.10. It is clear from the comparison that results from the numerical simulation of the static experiment are in very good agreement with the results from the MTS test.

High strain-rate experiments were performed on axisymmetric top hat specimen in Kolsky bar. Average strain rate during the experiment was 10^4 s^{-1}. Shear stress was calculated from the strain gage signal in the output bar using equation (3.9) and shear strain was calculated by integrating strain in the input bar as given by equations (3.4) and (3.5). Shear stress-strain curve thus obtained from the boundary measurements was compared with the results from MTS test and numerical simulation. Figure 3.10 shows the comparison between the shear stress-strain curves from different tests on top hat specimen. It can be observed that the stress-strain curve obtained from the Kolsky bar test matches closely with the MTS test, especially in the plastic region. This is expected from the rate insensitivity of the material used in the test. However, none of these curves match with the constitutive law of the material.

Again, it is evident that the stress-strain curve obtained from the experiments on the axisymmetric top hat specimen does not correspond to the constitutive law for the material, and finite element modeling of the experiment is necessary to predict the correct constitutive behavior of the material.

3.4.2 Axisymmetric H Specimen

Quasi-static and high strain-rate experiments were conducted on the axisymmetric H specimen. It was observed in the experiments that the stress concentration near the punch corners led to fracturing of the ligament instead of shearing. Thus, despite showing better results in finite element simulations, this specimen could not be used in the experiments. Meaningful stress-strain curve could not be obtained using this specimen.

3.4.3 Pinned Planar Specimen

Quasi-static experiments were carried out on plane specimen with pinned constraint (Fig. 3.6) at strain rate 10^{-2} s^{-1}. A photo-resist grid was deposited on one side of this specimen to observe the bending in the shear zone. It was observed that constraint reduced the bending of the arms of the plane specimen considerably. The square grid of photo-resist in the shear zone before the specimen was deformed is shown in Fig. 3.11. Fig. 3.12 shows the same grid after deformation. It can be clearly seen that not all the elements in this zone are equally sheared. There is a lot of shearing near both the corners and along the line joining the two corners. Considerable bending can be observed near the free surface in the shear zone where photo-resist starts developing cracks in a direction normal to the bending stress. Observation of fractured specimen showed that the crack ran diagonally from one corner of the shear zone to the other, along the line of maximum shear.

Shear stress-strain curve obtained from the boundary measurements of load and displacement is plotted in Fig. 3.13. Comparison with the constitutive law shows that this curve obtained from the load-displacement response of the specimen does not match

with the pure shear stress-strain curve for the material. Shear stress strain curve from the boundary measurements begins to exhibit nonlinearity at lower shear stress than the constitutive law; however, hardening exponent is almost the same in both the cases.

3.4.4 Plane Specimen with Lateral Constraint

Although the plane specimen with pinned constraint reduces bending considerably, it was noticed that there was some rotation of the specimen about the pins. Lateral constraint in the form of U-shaped block of tool steel reduced bending further and almost completely restricted the specimen from opening up from the base. Shear stress-strain curve obtained from quasi-static experiments is plotted in Fig. 3.14. The average strain rate during the test was 10^{-2} s^{-1}. Comparison with the shear stress-strain curve obtained from the numerical simulation of plane specimen without any constraint and fixed base shows that the two curves are close to each other. Thus, it can be concluded from these results that this constraint closely simulates fixed base boundary condition used in numerical simulations.

3.4.4 Plane Specimen with Built-in Constraint

The problem with using U-shaped block of tool steel as a constraint is that the assembly of the constraint and the specimen cannot be modeled exactly in numerical simulations. Also experimental results from high strain-rate Kolsky bar showed that the response of the structure could be affected because of the presence of constraint made from tool steel. The best constraint would be one, which is of the same material as the specimen and is an integral part of the specimen. This led to natural choice of plane specimen shown in Fig. 3.8. Since the whole specimen is fabricated from one piece of

aluminum, it can be modeled accurately using finite element analysis. First this specimen was subjected to quasi-static loading at shear strain rate 10^{-2} s^{-1} and shear stress-strain curve obtained from the load-displacement response was compared with that from the numerical simulation of the same geometry. These curves are plotted in Fig. 3.15. The two curves almost exactly match with each other.

High strain-rate Kolsky bar test was carried out on this plane specimen with the average shear strain rate 10^{4} s^{-1}. Shear stress-strain curve was constructed from the strain gage signals obtained from input and output bar. Fig. 3.16 shows this curve along with the curves from quasi-static MTS test and numerical simulations. All the three curves are in very good agreement with each other, but as expected from the numerical simulations all of them are different from the constitutive law for the specimen material. All the shear stress-strain curves obtained from the boundary measurements have lower yield stress as compared to the constitutive law, but hardening exponent for all the curves is almost the same. Also, as can be seen from the plots, high values of shear strain are achieved before specimen fractures. Shear stress-strain curve from SHPB test shows slight drop in load carrying capacity at shear strains greater than 1.1. This might indicate thermal softening of the material at high strain rates at high strains because of considerable rise in temperature in the shear zone.

It can be concluded that there is a good match between experimental and numerical results for plane specimen with built-in constraint. Since hardening exponent for all the curves is almost the same, correction can be made in the yield stress obtained from the boundary measurements to deduce the accurate constitutive law for the material (for details refer to Section 2.2.6). High values of shear strain (up to 1.5) at strain rates

above 10^4 s^{-1} can be obtained using this specimen. Also the planar geometry of this specimen makes the temperature measurement in the shear zone during the experiment possible.

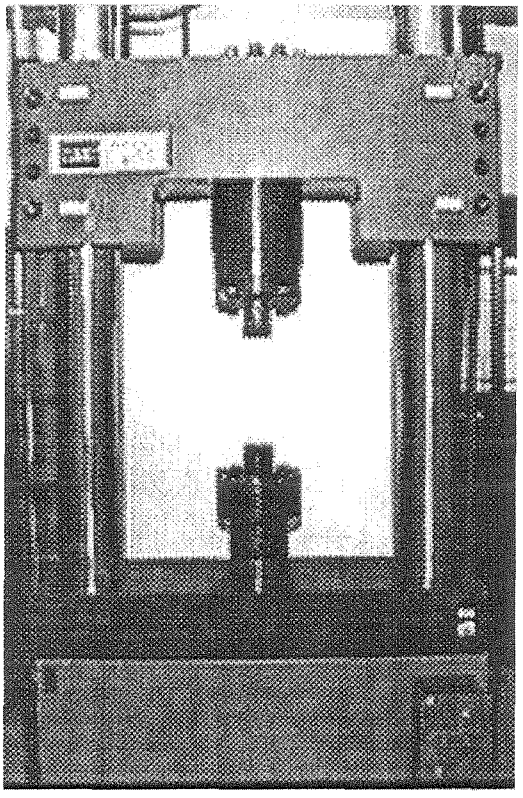

Figure 3.1 MTS machine

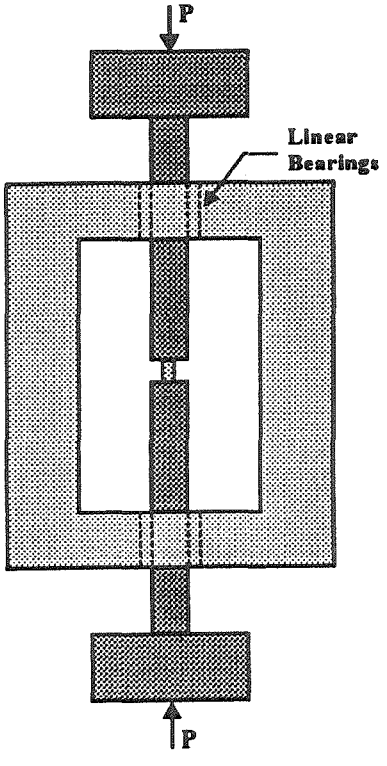

Figure 3.2 Alignment fixture

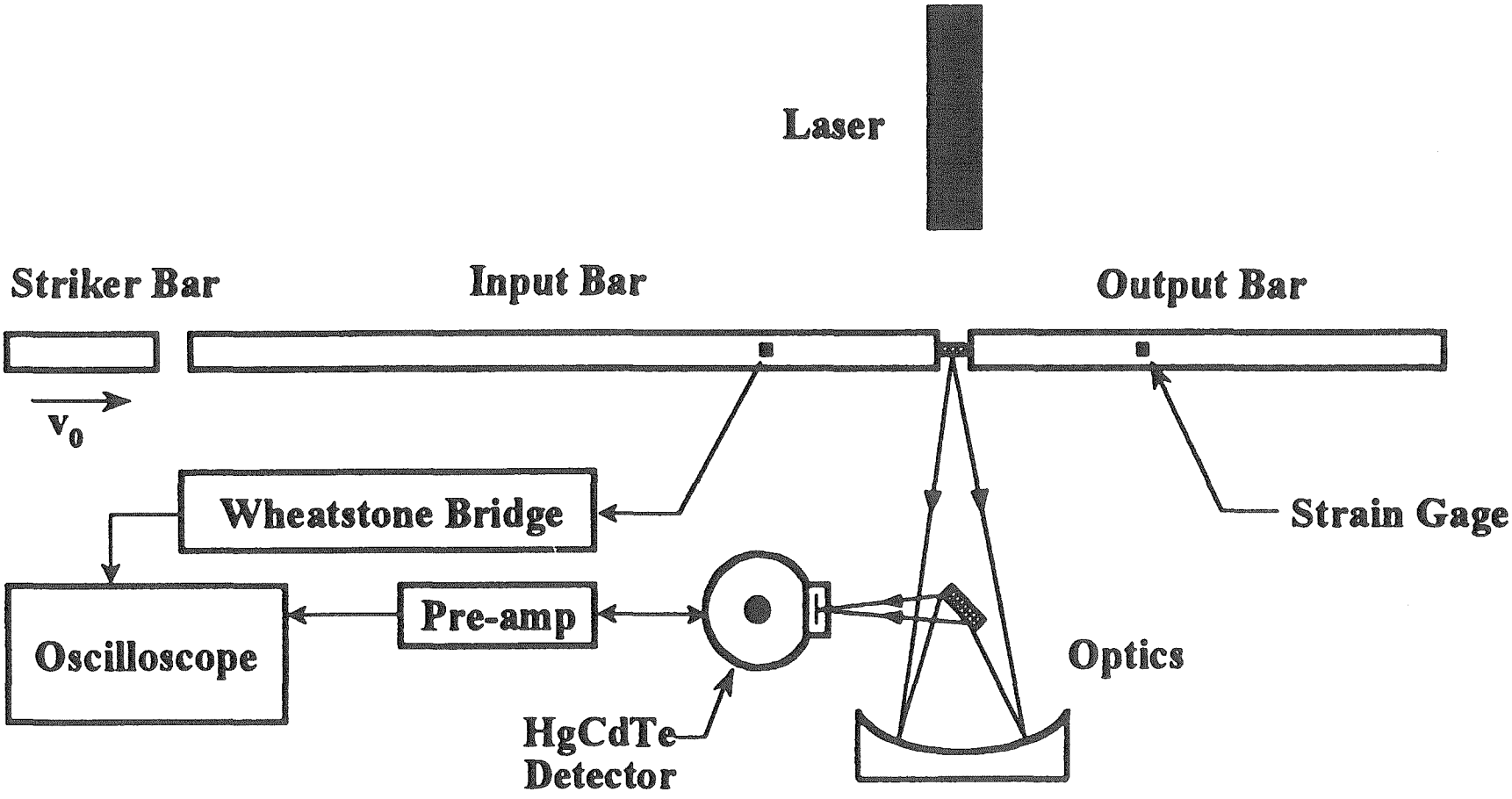

Figure 3.3 Kolsky bar in compression

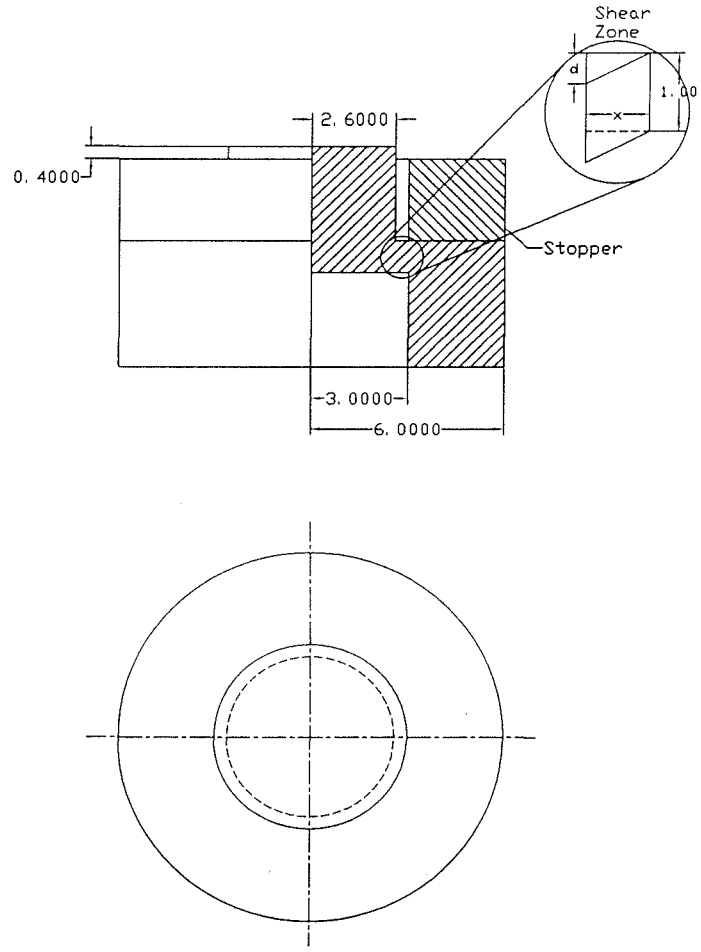

Figure 3.4 Engineering drawing of top hat specimen

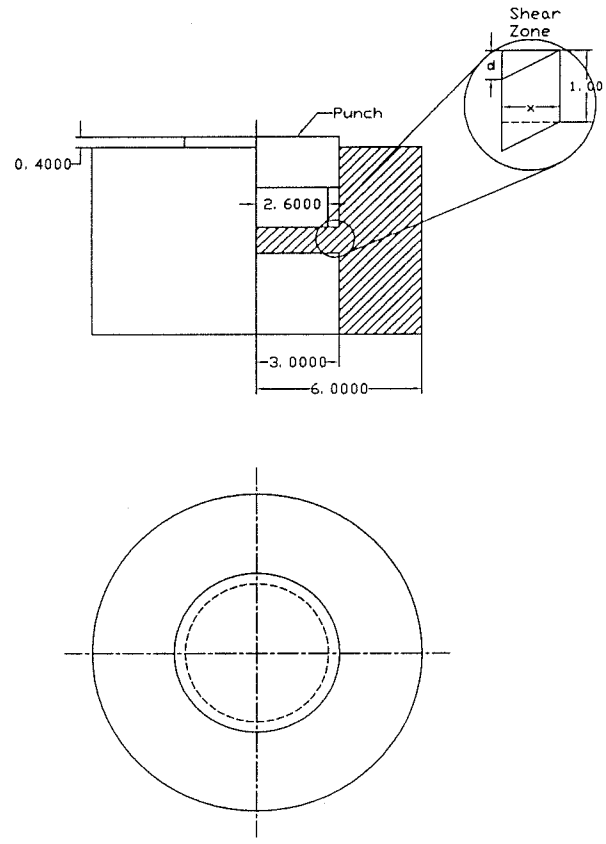

Figure 3.5 Engineering drawing of H specimen

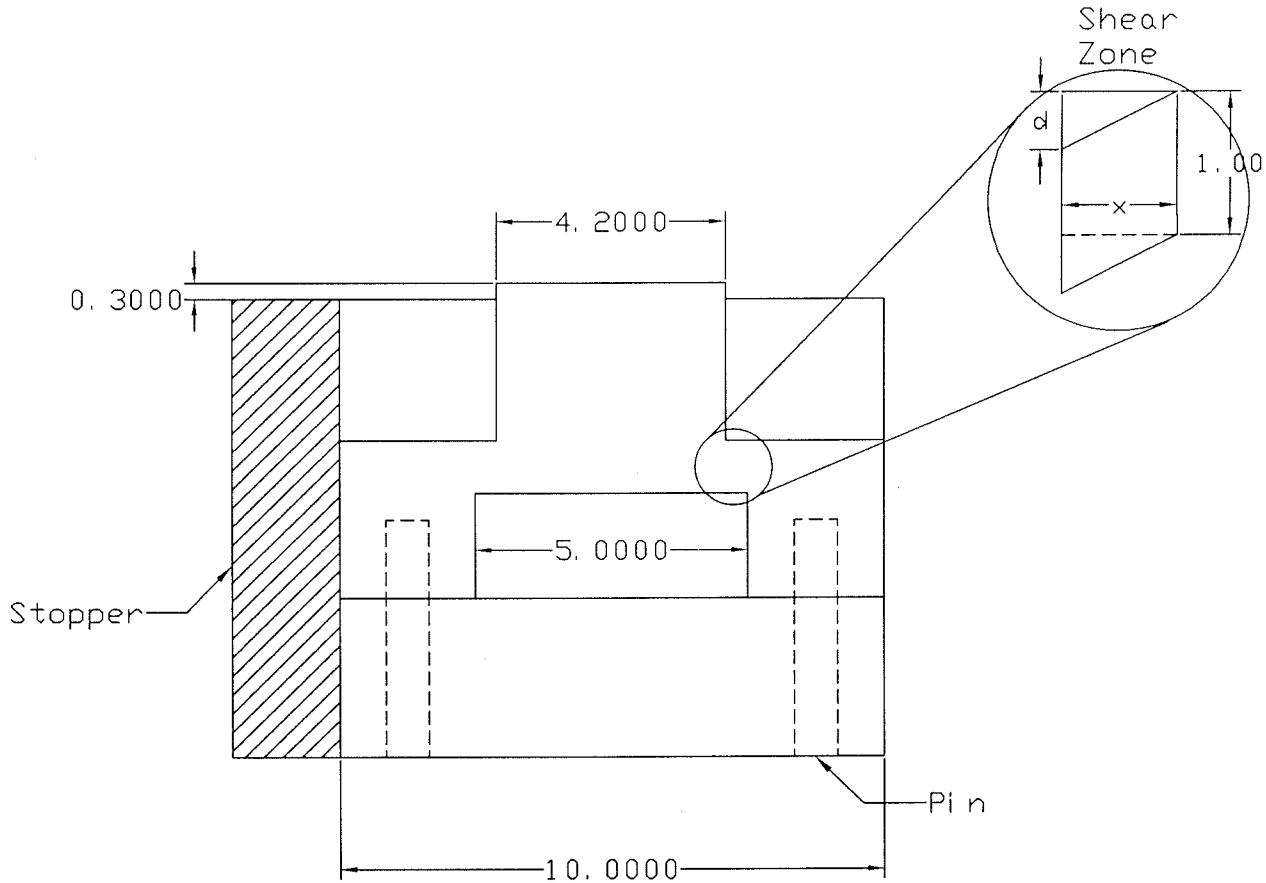

Figure 3.6 Pinned planar specimen

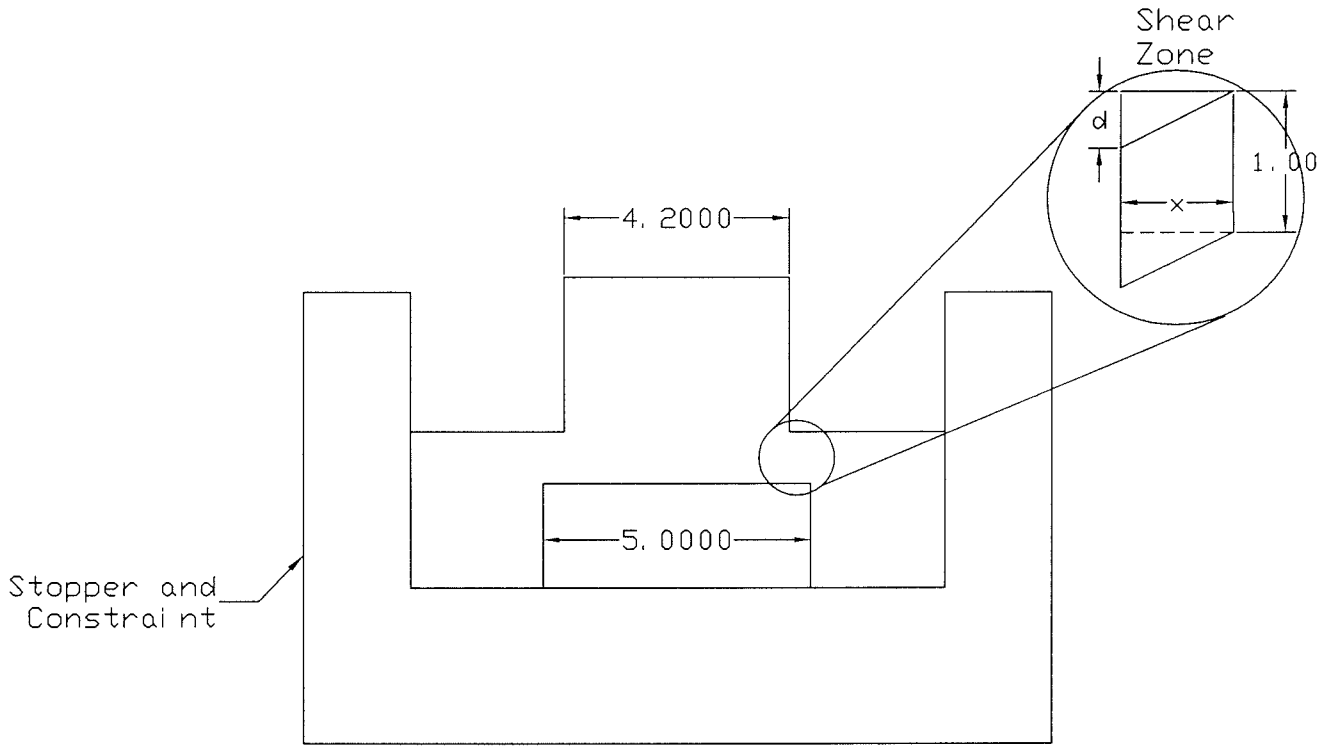

Figure 3.7 Plane specimen with lateral constraint

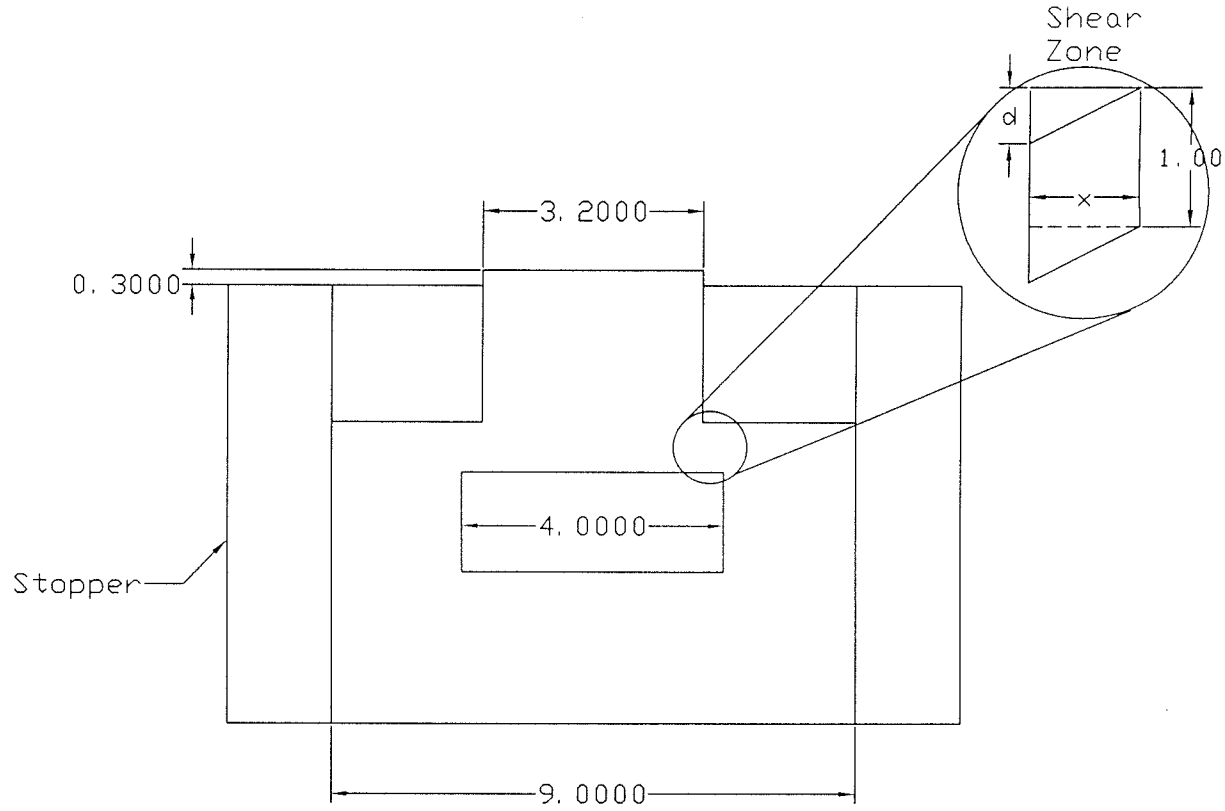

Figure 3.8 Plane specimen with built-in constraint

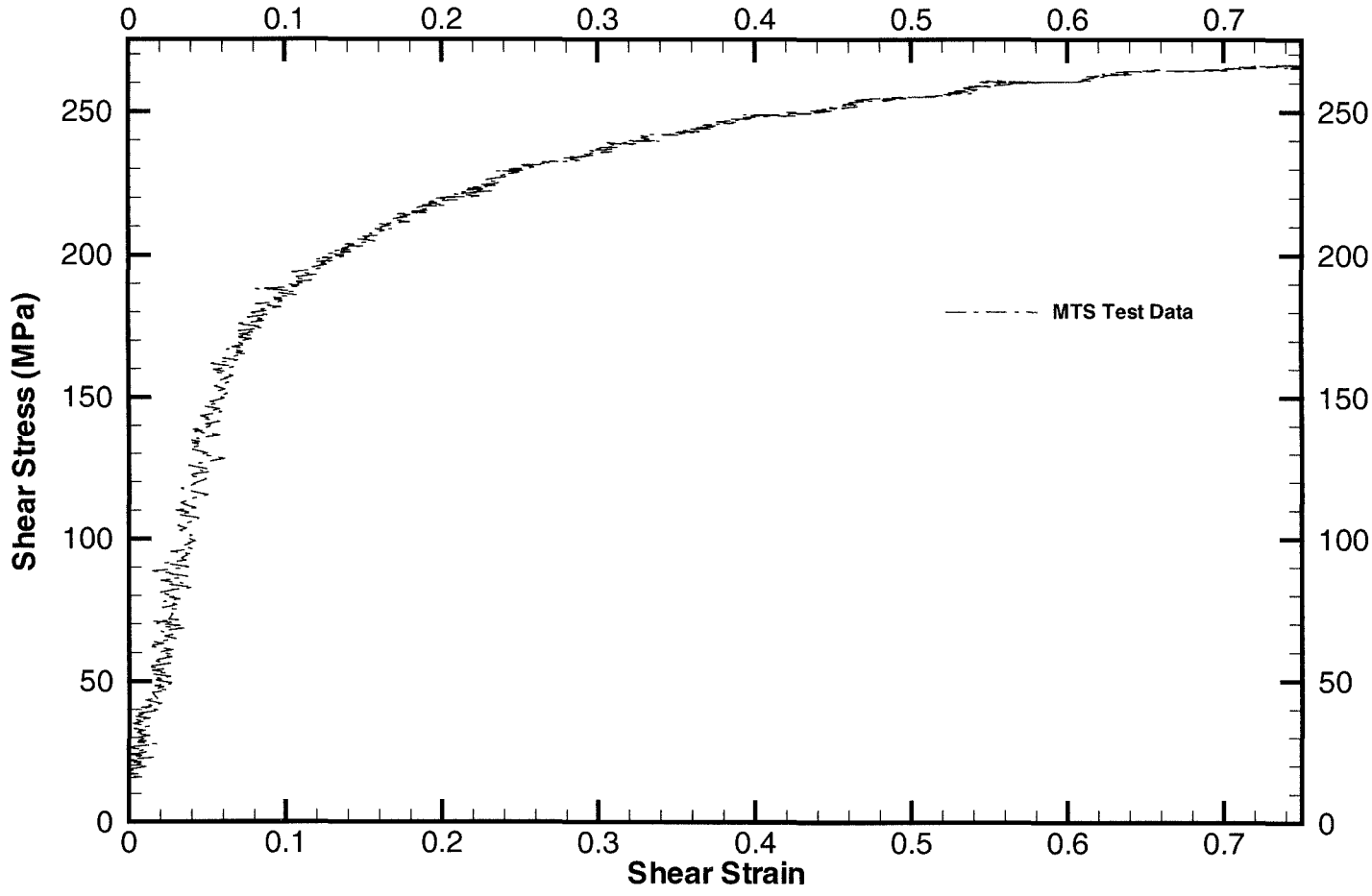

Figure 3.9 Shear stress-strain curve from quasi-static test on top hat specimen

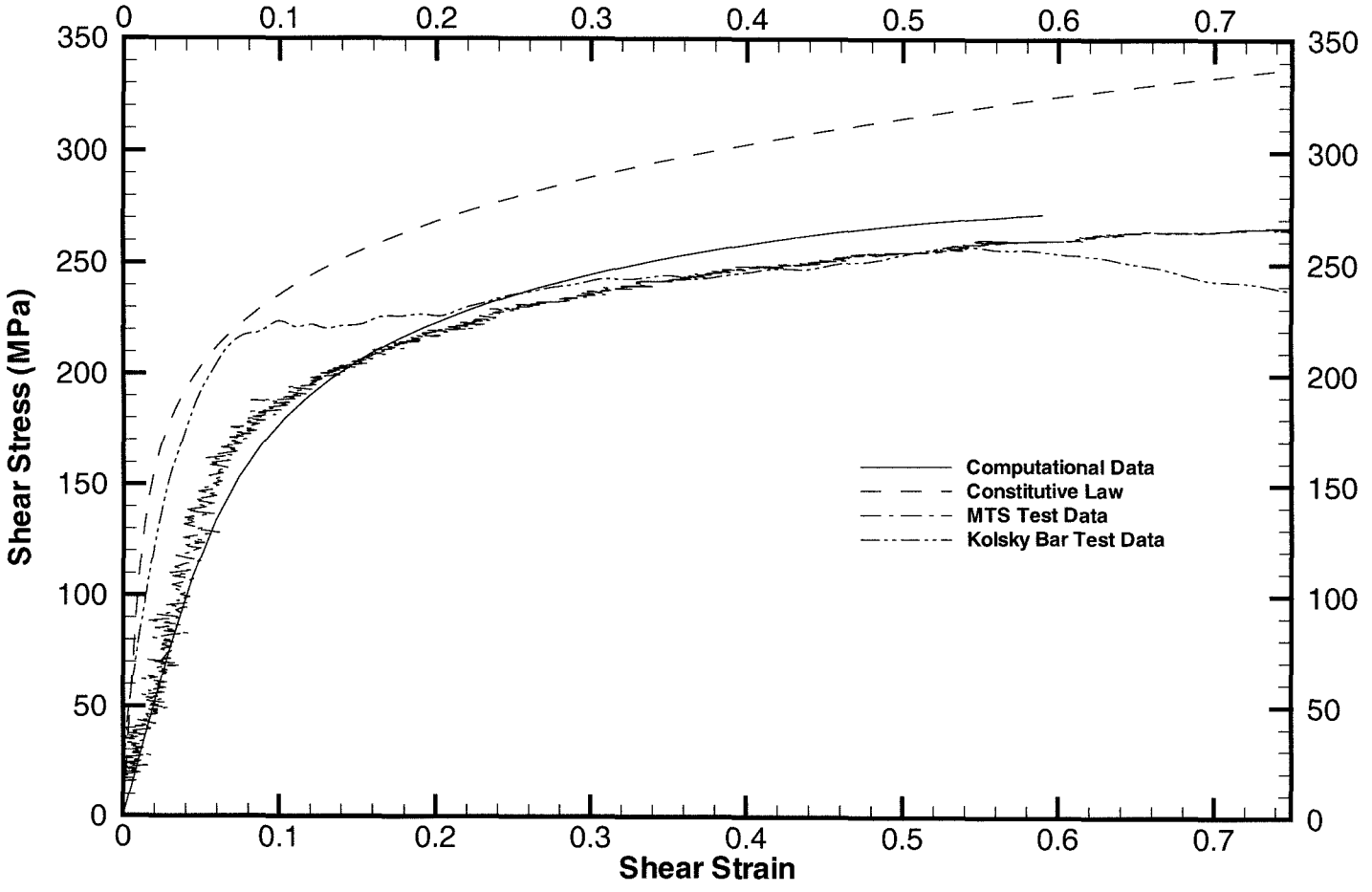

Figure 3.10 Comparison of shear stress-strain curve from experiments with the finite element results

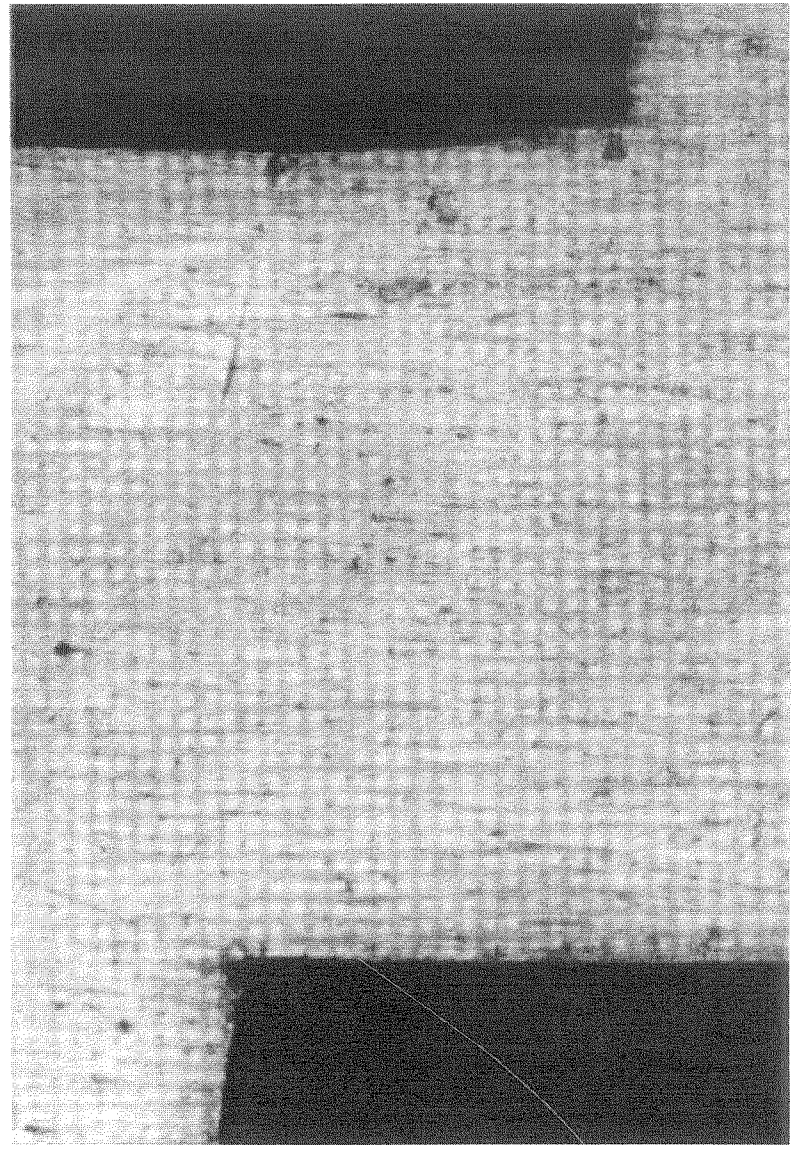

Figure 3.11 Photo-resist grid in shear zone before deformation

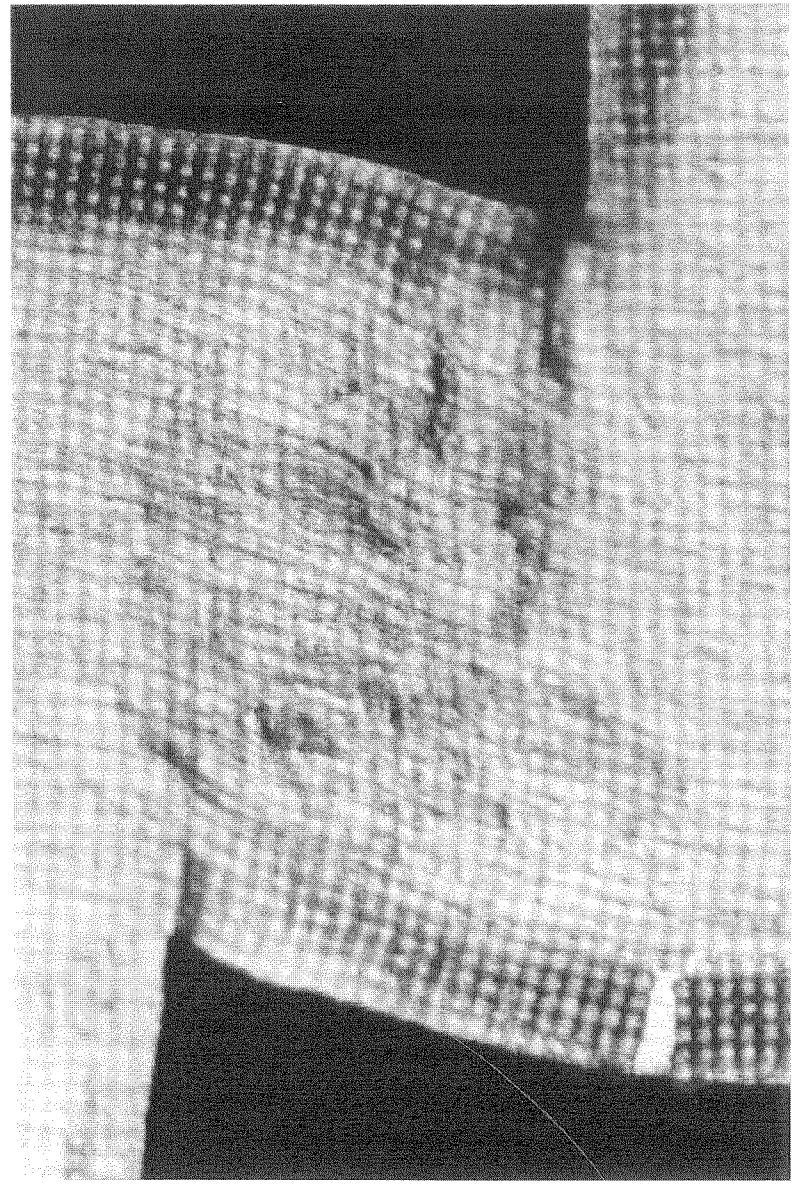

Figure 3.12 Photo-resist grid in shear zone after deformation

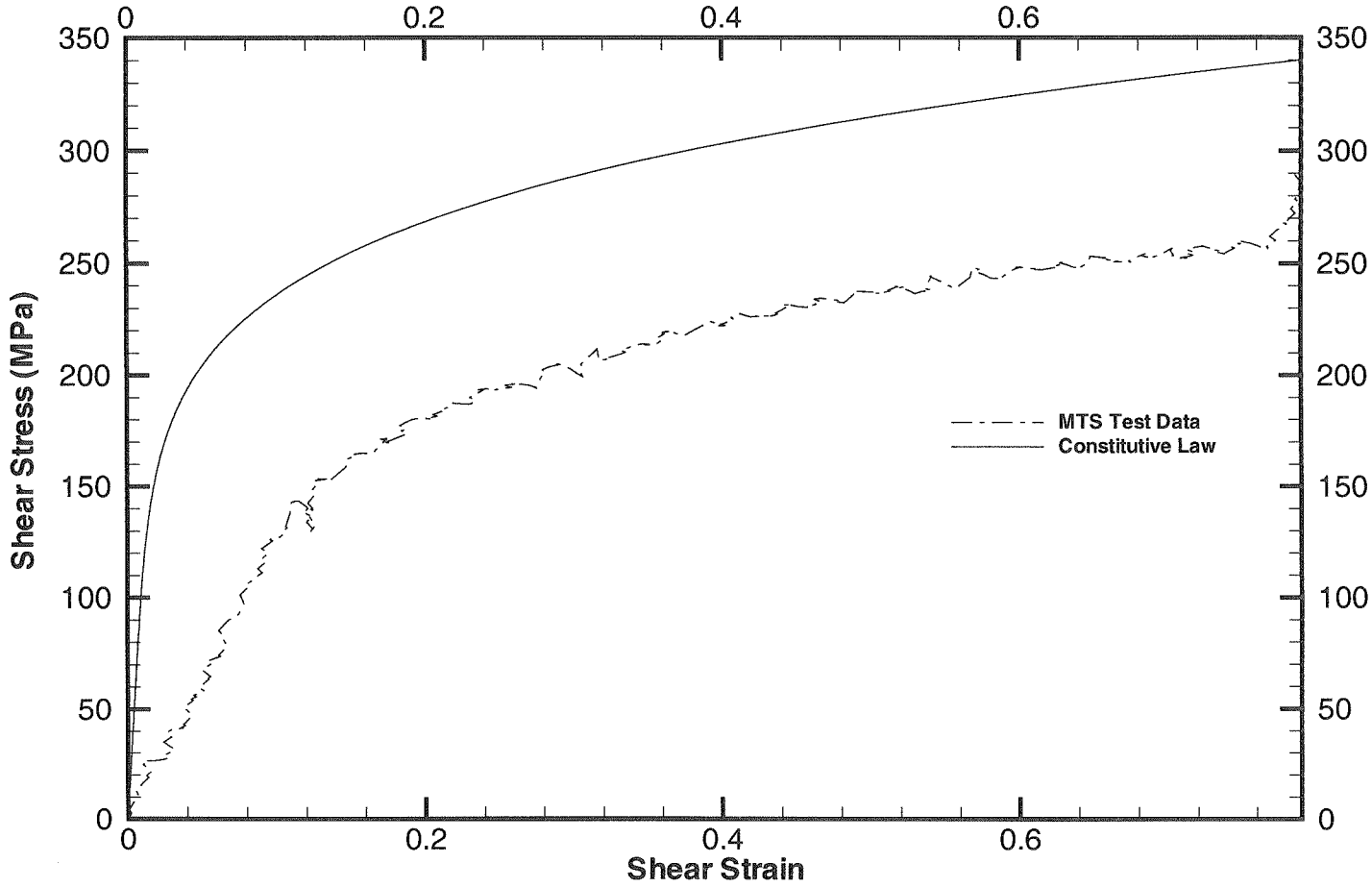

Figure 3.13 Comparison of experimental shear stress-strain curve and the constitutive law

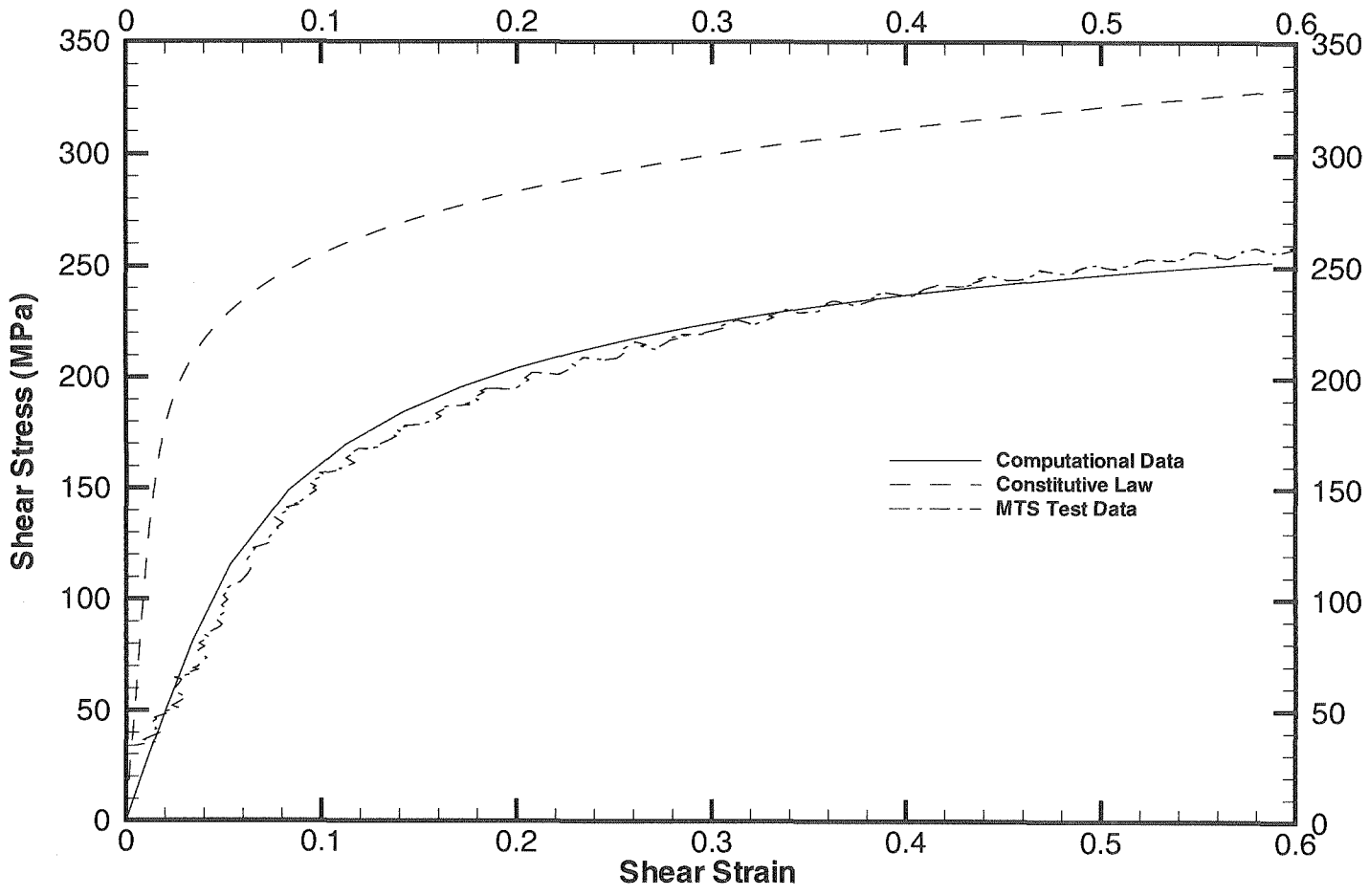

Figure 3.14 Experimental and numerical results for plane specimen with lateral constraint

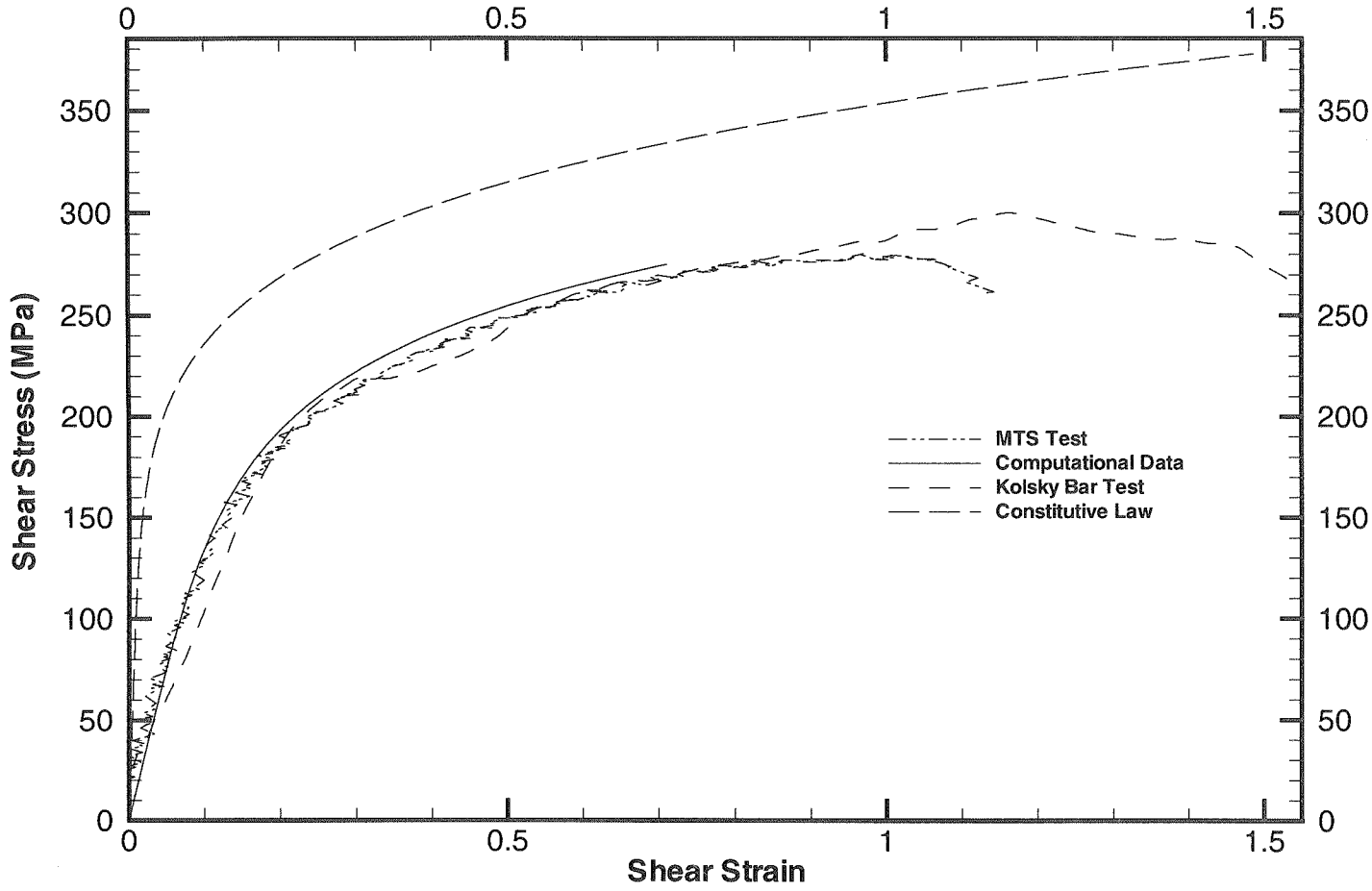

Figure 3.15 Experiment and numerical results for plane specimen with built-in constraint

Chapter 4

Conclusions and Future Work

4.1 Summary

Based on the numerical and experimental results, following conclusions can be made regarding the specimen geometry and the relationship between boundary measurements of stress-strain and constitutive law for the material.

- Numerical study of the axisymmetric top hat specimen used in literature to obtain shear stress-strain curve at high shear-strain rates was carried out using commercially available finite element software, ABAQUS. Considerable bending was observed in the shear zone and plastic deformation occurred near the corners of the shear zone because of stress concentration in that region. The state of stress in the shear zone was not that of a simple shear. The effect of these factors was reflected in the load-displacement response of the specimen and it was found that shear stress-strain curve from boundary measurement of load and displacement was consistently lower and did not match with the constitutive law used to model the specimen.
- New geometries were investigated using finite element simulations to study their load-displacement response. Discrepancy between the shear stress-strain curve obtained from boundary measurements and the constitutive law was less for the axisymmetric H specimen as compared to that for the axisymmetric top hat specimen. This specimen could not be used in experiments because it developed cracks in the early stages of deformation.

- A planar version of the axisymmetric top hat specimen was found suitable for making temperature measurements in the shear zone. Two types of external constraints were suggested to restrict the bending of the planar specimen. A plane specimen with built-in constraint made from a single block of material was found to be a better choice as compared to other plane specimens and axisymmetric top hat specimen. Built-in constraint made it easier to simulate this specimen using finite elements and also it provided more rigid constraint to avoid bending than other external constraints. This specimen was fabricated from one piece of aluminum using wire EDM.
- A relatively rate insensitive material, 2024-T3 aluminum, was investigated with all the specimen geometries. Material Test System (MTS) was used to conduct experiments at low strain rate, 10^{-2} s^{-1}, whereas high strain rate experiments were carried out on Kolsky compression bar at strain rates 10^{4} s^{-1}. Experimental results from both the experiments were compared against each other and also the numerical results. Quasi-static and high strain-rate response of the axisymmetric top hat specimen was almost the same, verifying the rate insensitivity of the material. Also these results matched with the numerical results for the static loading of the top hat specimen. Experimental and numerical results for the plane specimen with external constraint were in good agreement with each other. The best agreement between the different curves was seen for the plane specimen with the built-in constraint. Very high shear strains (~1) were reached in the high strain-rate experiments on this specimen. Some amount of thermal softening was observed at high strain rates at higher shear strains.

- In all the experiments and numerical study, shear stress-strain curve obtained from the boundary measurements of load and displacements was found to be different from the constitutive law for the material. Thus, it was concluded that both the experimental and numerical study is necessary in order to obtain the constitutive law for the material in shear.

4.2 Future Work

Based on the numerical and experimental study of high-strain-rate shearing behavior of metals, the following suggestions are made for future work.

- Following the method developed in this study, experiments should be carried out on rate dependent materials at strain rates ranging from 10^4 s^{-1} to 10^5 s^{-1}. Planar top hat specimen with built-in constraint can be used in experiments with the standard Kolsky bar configuration to achieve these strain rates. Both numerical and experimental study is necessary in order to obtain accurate constitutive behavior of the material.
- Temperature measurements should be made in the shear zone using infrared temperature detector. This provides additional information to construct complete thermomechanical model of metals.
- Numerical simulations of the experiments with rate dependent material model and thermal softening should be carried out using commercially available finite element software. This information can then be used to evaluate the constitutive behavior of strain-rate dependent metals such as titanium.
- The objective would be then to use a constitutive law in the numerical simulations that will reproduce the experimental data such as load and displacement at the

boundary and temperature rise in the shear zone. This constitutive law would then represent the accurate behavior of the material under shear as a function of strain, strain-rate and temperature.

- Experiments and numerical simulations can be conducted at low strain rates at which the constitutive behavior is known from other tests. The data from these tests can be used as a reference to predict the stress-strain curve at higher strain rates for which data is not available.
- To study the constitutive behavior of metals at elevated temperature, experiments should be carried out at high temperature by heating the specimen.
- It is important to subject the specimen to constant strain rate to study the rate sensitivity of the material. Direct impact of the striker bar on the specimen should be used in order to reduce the rise time of incident pulse in the input bar of the Kolsky compression bar. This technique requires an additional setup to measure the impact velocity of the striker bar.

References

Andrade, U., Meyers, M. A., Vecchio, K. S. and Chokshi, A. H. (1994), "Dynamic Recrystallization in High-strain, High-strain-rate plastic Deformation of Copper," *Acta Metall. Mater.*, **42**, 3183.

ASM Handbook: Vol. 8 (1995), "Mechanical Testing," ASM International, Metals Park, OH.

Beatty, J. H., Meyer, L. W., Meyers, M. A. and Nemat-Nasser, S. (1991), "Formation of Controlled Adiabatic Shear Bands in AISI 4340 High Strength Steel," *12th Army Symposium on Solid Mechanics,* Plymouth, MA.

Chung, D. T., Moon, S. K. and Yoo, Y. H. (1994), "Numerical and Experimental Study of the Formation of Adiabatic Shear Band," *Journal de Physique,* **4**, 547.

Follansbee, P. S. (1985), "The Split Hopkinson Bar," in *ASM Handbook:* 9th Edition, **8**, ASM International, Metals Park, OH.

Hodowany, J., (1997), "On the Conversion of Plastic Work into Heat," *Ph.D. Thesis,* California Institute of Technology, Pasadena, CA.

Klepaczko, J. R. (1994), "An Experimental Technique for Shear Testing at High and Very High Strain Rates. The Case of a Mild Steel," *Int. J. Impact Eng.*, **15**, 25.

Kolsky, H. (1949), *Stress Waves in Solids,* Dover Publications, New York.

Lindholm, U. S. (1964), "Some Experiments With the Split Hopkinson Pressure Bar," *J. Mech. Phys. Solids,* **12**, 317.

Marusich, T. D. and Ortiz, M. (1995), "Modeling and Simulation of High Speed Machining," *Int. J. for Numerical Methods in Engineering,* **38**, 3675.

Meyer, L. W., Hartman, K. H. and Kunze, H. D. (1981), in *Shock Waves and High-Strain-Rate Phenomena in Metals,* Plenum Press, New York, 325.

Meyers, M. A. (1994), *Dynamic Behavior of Materials*, Wiley-Interscience publication, New York.

Meyers, M. A., Andrade, U. R. and Chokshi, A. H. (1995), "The Effect of Grain Size on the High-Strain, High-Strain-Rate Behavior of Copper," *Metall. & Mater. Trans. A.,* **26A**, 2881.

Vecchio, K. S. (1994a), "High-Strain, High-Strain-Rate Deformation of Tantalum and Tantalum-Tungsten Alloys," *Journal de Physique,* **4**, 301.

Vecchio, K. S. and Chen, R. W. (1994b), "Microstructural Characterization of Shear Band Formation in Al-Li Alloys," *Journal de Physique,* **4**, 459.

Zehnder, A. T. and Rosakis, A. J. (1991), "On the Temperature Distribution at the Vicinity of Dynamically Propagating Cracks in 4340 Steel," *J. Mech. Phys. Solids,* **39**, 385.

Zhou, M. and Minnaar, K. (1998), "Analysis of the Dynamic Shear Failure Resistance of Structural Metals," to appear in *J. Mech. Phys. Solids.*